Geol. Mag. **147** (3), 2010, pp. 451–468. © Cambridge University Press 2009
doi:10.1017/S0016756809990707

Petrology and geochemistry of the orbicular granitoid of Sierra de Velasco (NW Argentina) and implications for the origin of orbicular rocks

PABLO GROSSE*†, ALEJANDRO J. TOSELLI‡ &JUANA N. ROSSI‡

*CONICET & Fundación Miguel Lillo, Miguel Lillo 251, (4000) San Miguel de Tucumán, Argentina
‡Instituto Superior de Correlación Geológica – CONICET & Facultad de Ciencias Naturales, Universidad Nacional de Tucumán, Miguel Lillo 205, (4000) San Miguel de Tucumán, Argentina

(*Received* 7 May 2009; *accepted* 23 September 2009; First published online 15 December 2009)

Abstract – The Velasco orbicular granitoid is a small (65 × 15 m), irregularly-shaped body that crops out within the Huaco granite, central Sierra de Velasco, NW Argentina. It consists of ellipsoid-shaped orbicules of 3 to 15 cm length immersed in an aplitic to pegmatitic matrix. The orbicules are formed by a core made up of a K-feldspar megacryst, partially to totally replaced by plagioclase, an inner shell of radial and equant plagioclase crystals, a layer of tangentially oriented biotite laths, and an outer shell of plumose plagioclase crystals, containing diffuse rings of tangentially oriented biotite. The orbicular granitoid formed *in situ* in a pocket of evolved and volatile-rich melt segregated from the surrounding partially crystallized Huaco granite, possibly via a filter pressing mechanism. The segregated melt entrained relatively few K-feldspar megacrysts into the pocket, leaving behind a concentration of megacrysts around the pocket. High water concentration caused effective superheating of the melt and destruction of nuclei, with only the large megacrysts surviving as solids. Sudden water-pressure loss and exsolution of the volatile phase, perhaps related to a volcanic eruption or fracturing of the surrounding granite, caused rapid undercooling of the melt. The orbicules grew in the undercooled melt by heterogeneous nucleation on the megacrysts, which acted as nucleation seeds, and crystallization of reversely zoned radial plagioclase and sporadic crystallization of tangential biotite rings according to fluctuations in its saturation. Orbicular growth gave way to crystallization of the equiaxial inter-orbicular matrix in two stages, when sufficient polymerization of the melt was attained. The time scale of formation of the orbicular granitoid was fast, possibly a matter of a few weeks or months.

Keywords: orbicular granitoid, plumose plagioclase, reverse zoning, Huaco granite, Sierra de Velasco, Argentina.

1. Introduction

Orbicular rocks are a very unusual rock type notable for their concentric rings of radially- and tangentially-oriented minerals. The worldwide scarcity and small size of orbicular rock outcrops probably reflects very specific conditions during their formation. Although a magmatic origin is generally not questioned, the mechanisms and conditions required for their formation are still not well constrained.

Since the beginning of the 20th century, several studies of orbicular rocks have been carried out. Some of the more relevant contributions are those of Sederholm (1928), Eskola (1938), Goodspeed (1942), Grolier (1961), Quartino & Villar Fabre (1962), Leveson (1963, 1966), Moore & Lockwood (1973), Enz, Kudo & Brookins (1979), Brigham (1983), Elliston (1984), Vernon (1985), Symes, Bevan & Qasim (1987), Yazgan & Mason (1988), Owen (1991), Ort (1992), Sinclair & Richardson (1992), Decitre, Gasquet & Marignac (2002), Durant & Fowler (2002), Lahti (2005), Lindh & Näsström (2006) and Tagiri, Oba & Fujinawa (2007). In Argentina, four orbicular rock settings have been studied. Quartino & Villar Fabre (1962), and later Linares & Quartino (1978), studied the orbicular granitoid of Sierra de Velasco, which is the subject of the present contribution. Two other orbicular rocks crop out in the sierras of Córdoba: an orbicular granite, described by Sureda & Viramonte (1972), and an orbicular cordieritite, studied by Gordillo (1979) and Rapela *et al.* (2002). The fourth setting is of orbicules within the Cerro Panizos ignimbrites and lavas in the Puna Plateau of the Central Andes (Ort, 1992) and is the only detailed study of orbicular volcanic rocks.

A review of the existing literature establishes the general characteristics of orbicular rocks: (1) they have an 'orbicular' structure, that is, concentric radially- and tangentially-oriented mineral shells surrounding a core; (2) they consist of 'orbicules' immersed in an 'inter-orbicular' matrix; (3) they form irregularly shaped bodies generally on a scale of tens to hundreds of metres; (4) the host rock is almost always igneous, though its composition can vary considerably; the more common rock types are granite, granodiorite, diorite and gabbro; (5) they are found mainly in marginal parts of igneous bodies; (6) the orbicules are typically

†Author for correspondence: pablogrosse@yahoo.com

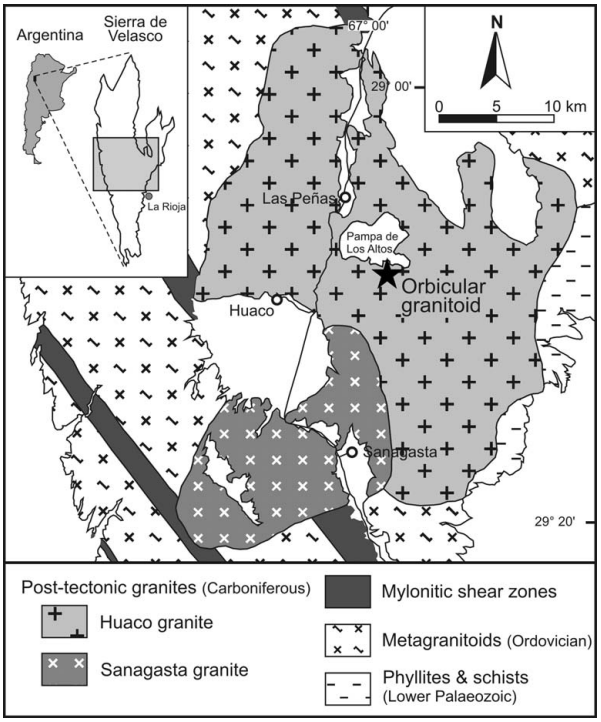

Figure 1. Simplified geological map of central Sierra de Velasco, NW Argentina, showing location of the Velasco orbicular granitoid (black star). Modified from Grosse *et al.* (2009).

spheroidal to ellipsoidal, although they can also have irregular shapes and be fragmented or deformed; (7) the size of the orbicules varies from a few centimetres to ~ 35 cm; (8) the orbicules can be grouped, in contact with one another, or occur as discrete bodies within the matrix; (9) orbicules can either be proto-orbicules, defined as a core partially surrounded by a poorly defined shell, orbicules with one shell, or orbicules with multiple shells (Leveson, 1966); (10) the cores can consist of portions of the enclosing rock, xenoliths, mineral aggregates or individual crystals (usually feldspar); (11) the concentric shells are typically of feldspar (K-feldspar or plagioclase), biotite and/or amphibole, but can also contain quartz, pyroxene, tourmaline, cordierite, etc.; (12) the inter-orbicular matrix can have a variable composition and texture (granitic, pegmatitic, dioritic, etc.) that is either similar to or different from the host rock; (13) orbicular rocks are commonly associated with layered igneous rocks, comb-layered structures, megacrysts, xenoliths and mineral segregations.

This article deals with an orbicular granitoid located in the Sierra de Velasco, La Rioja province, NW Argentina (Fig. 1). It is possibly the best preserved orbicular rock outcrop in Argentina, and is a rare case where the outcrops reveal the relations with the host rock. Quartino & Villar Fabre (1962) first studied this orbicular rock, carrying out field and petrographic descriptions. Here, we present the results of a new and thorough field, petrographic and geochemical study of the Velasco orbicular granitoid. We then discuss how the orbicular granitoid formed and propose a genetic model, recognizing some of the key factors in the formation of orbicular rocks.

2. Local geological setting: the Huaco granite

The Velasco orbicular granitoid is located within the Huaco granite (Fig. 1). The Huaco granite is a large granitic massif that crops out in central Sierra de Velasco (Fig. 1) and is part of the abundant Palaeozoic magmatism characteristic of the Sierras Pampeanas geological province of NW Argentina. This granite, and the Sanagasta granite to the southwest, are post-tectonic granites that intrude into Lower Palaeozoic phyllites and schists, Ordovician metagranitoids and mylonitic shear zones of possible Devonian age (Fig. 1). The Huaco granite is of Early Carboniferous age (350 ± 11 Ma and 358 ± 10 Ma, U–Pb on monazite: Grosse *et al.* 2009; 349 ± 5 Ma, LA-ICP-MS U–Pb on zircon: Söllner *et al.* 2009).

The Huaco granite is a strongly porphyritic, biotite–muscovite syeno- to monzogranite. It consists of abundant (30–35 vol. %) perthitic K-feldspar megacrysts set in a medium- to coarse-grained groundmass of anhedral quartz (25–40 %), subhedral plagioclase laths (15–30 %), interstitial perthitic K-feldspar (2–15 %), biotite (4–10 %) and muscovite (2–6 %). Accessory minerals include apatite, zircon, monazite and ilmenite.

The megacrysts of the Huaco granite are commonly oriented, defining a primary magmatic foliation. Their size varies between 1 and 10 cm (length of main axis), with an average size of 2.7 ± 0.4 cm. They have a magmatic origin, following the criteria of Vernon (1986). A crystal size distribution (CSD) study carried out by P. Grosse (unpub. Ph.D. thesis, Univ. Córdoba, 2007) suggests that the megacrysts formed by a textural coarsening process (e.g. Marsh, 1988; Higgins, 1999).

Pegmatites and aplites are common in the Huaco granite. The larger pegmatites are generally zoned and form irregular- to globular-shaped bodies up to 30 m thick and 200 m long. They are of the rare-element type, commonly containing beryl, phosphates and Nb–Ta oxides (Galliski, 1993; Sardi, 2005; Sardi & Grosse, 2005).

The Huaco granite is silica- (70.6–74.7 %) and potassium-rich (4.8–5.8 %), alkali-calcic, ferroan and moderately peraluminous (Alumina Saturation Index = 1.06–1.18). Further details concerning the petrology, geochemistry and geochronology of this granite can be found in Grosse *et al.* (2009).

3. Field relations and petrography

The orbicular granitoid crops out along a small N–S-oriented gully a few kilometres south of the Pampa de Los Altos, in the central part of the Huaco granite (Fig. 1). The orbicular body has an irregular shape consisting of a main N–S-oriented segment of 65 × 15 m and a smaller 35 × 5 m segment that branches out toward the NE (Fig. 2). The body is in contact with the

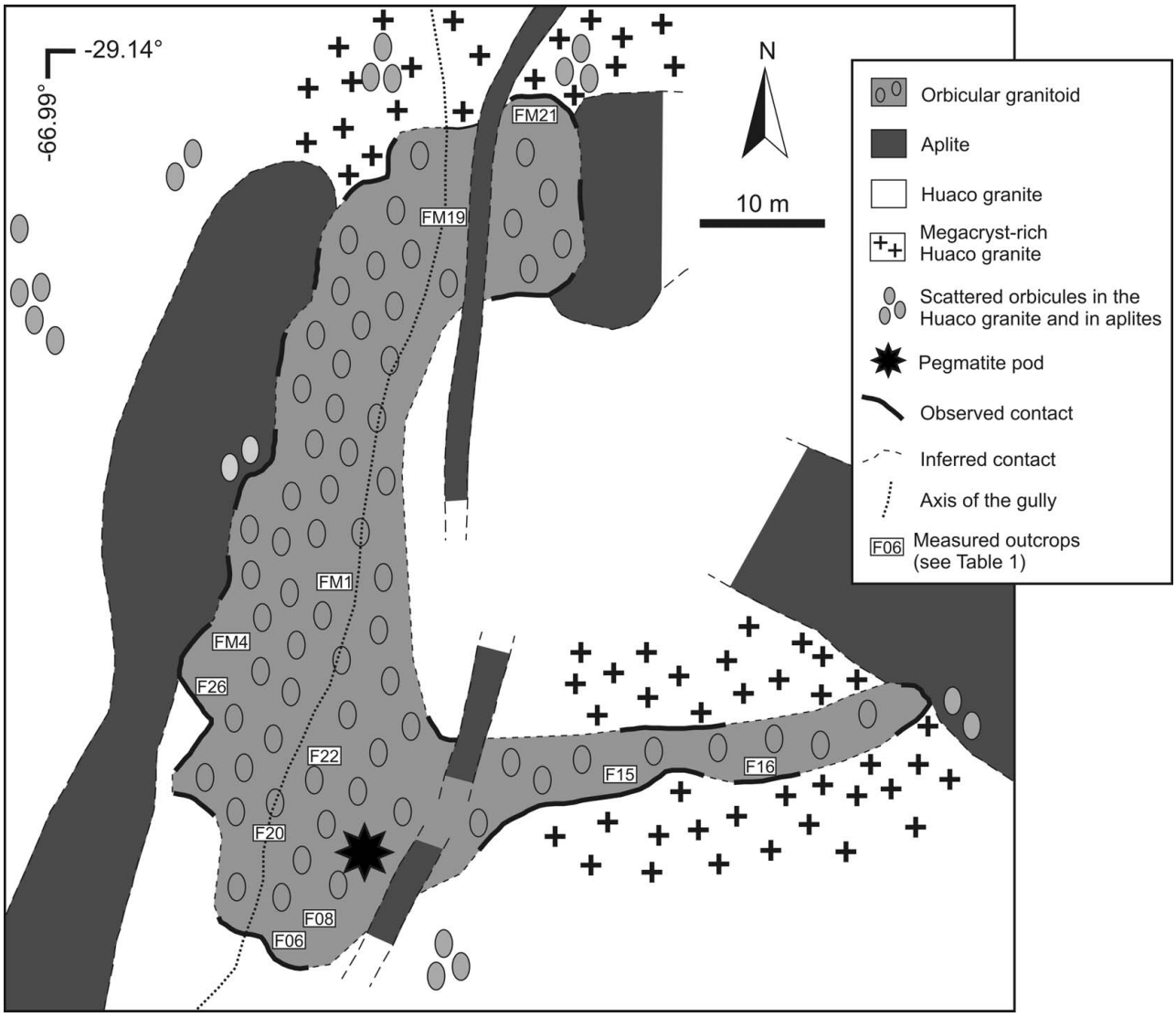

Figure 2. Geological map of the Velasco orbicular granitoid.

Huaco granite and with several aplitic dykes (Fig. 2). The Huaco granite is the host rock of the orbicular granitoid, whereas the aplitic dykes cross-cut both the Huaco granite and the orbicular granitoid (Fig. 2).

In general, the Huaco granite that crops out around the orbicular granitoid is similar to the porphyritic granite described in Section 2. However, the granite bordering the orbicular granitoid shows a strong increase in the abundance of K-feldspar megacrysts in several places (Fig. 2), in some cases forming 'cumulates' made up almost exclusively of megacrysts. The contact between the Huaco granite and the orbicular granitoid is generally sinuous and sharp (Fig. 3), although it can be somewhat gradational due to the presence of orbicules in the Huaco granite (Fig. 3b). Additionally, in many places around the orbicular body, the Huaco granite contains isolated orbicules (Figs 2, 4), which are mostly similar to the orbicules of the main body, but also include some very small proto-orbicules (Fig. 4, inset).

The abundance of aplites close to and in contact with the orbicular body is much greater than is normal in the Huaco granite. These aplites form decimetre-thick dykes and irregularly-shaped bodies (Fig. 2). They have a fine-grained equigranular texture and are composed of quartz, K-feldspar, plagioclase, muscovite and biotite. Rarely, they contain scattered orbicules.

The orbicular granitoid has a conglomeratic appearance and consists of ellipsoidal orbicules immersed in a variably-grained inter-orbicular matrix (Fig. 5). Based on 11 measured outcrops, the proportion of orbicules varies between 49 and 66 %, with an average of 58 % (Table 1). There is no systematic variation in the orbicule–matrix proportion from centre to margins of the body, or from one sector to another.

The orbicules have ellipsoidal shapes with average axial ratios of 2.0:1.4:1.0. They are completely immersed in the matrix or in contact with each other (Fig. 5). The size of the orbicules varies between 3 and 15 cm (length of the main axis), exceptionally reaching up to 20 cm. Two types of outcrops can be distinguished, outcrops with 'normal' sized orbicules and outcrops that contain only small orbicules (Table 1; Fig. 5). In the eight 'normal' outcrops measured, the

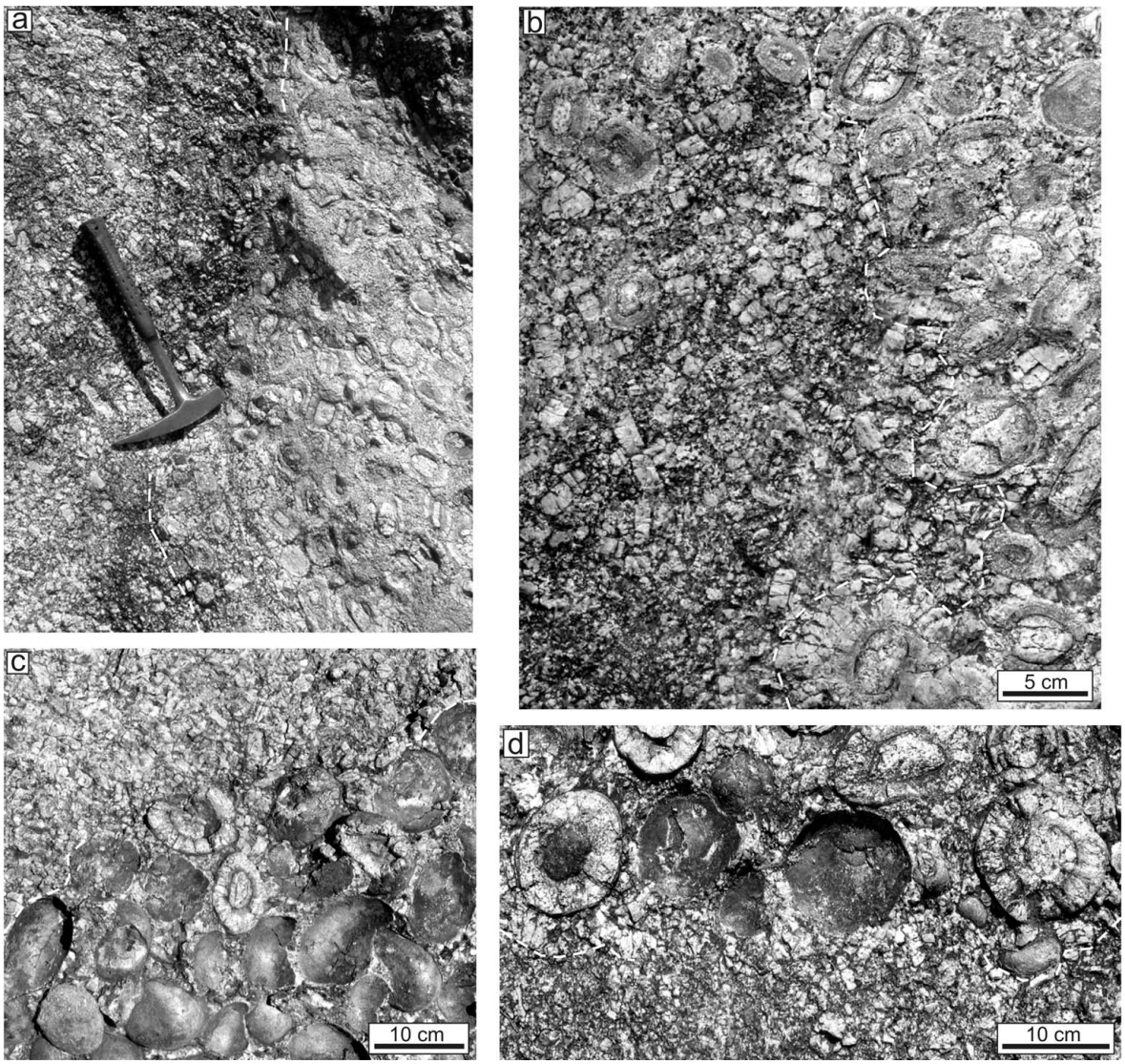

Figure 3. Outcrops showing the contact between the Velasco orbicular granitoid and the enclosing Huaco granite. In (a) hammer length is 28 cm. Note in (b) the scattered orbicules in the Huaco granite.

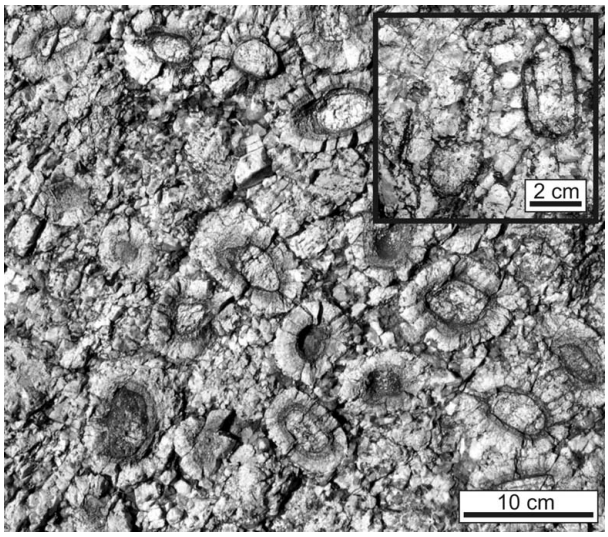

Figure 4. Orbicules and proto-orbicules (inset) scattered within the Huaco granite in outcrops around the Velasco orbicular granitoid.

Table 1. Abundance and size of orbicules measured on 11 outcrops

Outcrop	Number of orbicules	Abundance of orbicules (%)	Minimum length (mm)	Maximum length (mm)	Average length (mm)
F06	13	57	57	98	78
F08*	28	50	25	60	39
F15	53	49	31	126	77
F16	12	64	50	114	87
F20*	31	59	27	68	47
F22	12	63	64	102	81
F26*	17	57	34	74	56
FM01	19	65	51	135	90
FM04	30	56	25	133	91
FM19	9	66	55	109	80
FM21	12	50	49	98	76

*Outcrops with only small orbicules. For location of all outcrops see Figure 2.

size of the orbicules varies between 2.5 and 13.5 cm. The most abundant size-interval is 9–10 cm (18 %), and 80 % of the orbicules have sizes between 5 and 11 cm. In the three measured outcrops with small

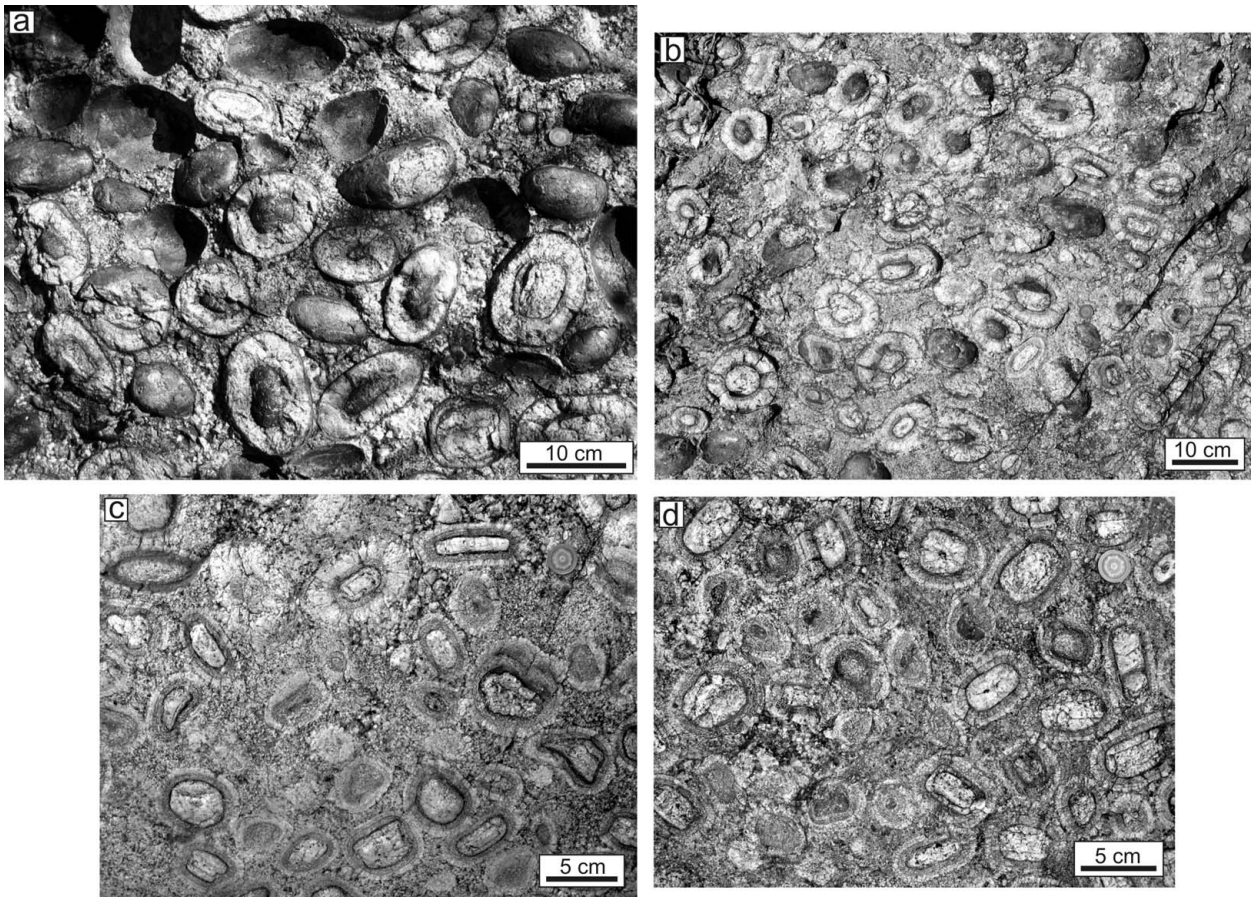

Figure 5. Outcrops of the Velasco orbicular granitoid. (a) and (b) correspond to 'normal' outcrops, while (c) and (d) are of outcrops with small orbicules.

orbicules, the size of the orbicules varies between 2.5 and 7.4 cm, with an average size of 4.6 cm. The outcrops with small orbicules are found in different parts of the orbicular body, both in border and central areas. The transition towards normal outcrops with larger orbicules is typically sharp.

The orbicules have grey-coloured, smooth and dull outer surfaces, but they show striking inner structures consisting of a core surrounded by several concentric shells (Fig. 6a). The inner structure of the orbicules can be divided into core, inner shell, dark layer and outer shell. In addition, the outer shell generally contains an inner and an outer diffuse band (Fig. 6b). The thickness and the proportions of each one of these zones can vary considerably (Fig. 6a). The smaller orbicules commonly have a core and only one shell (Fig. 6a).

The core consists of a K-feldspar perthitic megacryst partially or totally replaced by plagioclase (Figs 6a, 7). The relict K-feldspar rarely forms patches with simultaneous extinction and pericline–albite twinning. The plagioclase shows incomplete polysynthetic twinning that follows the K-feldspars' pre-existing structure (Quartino & Villar Fabre, 1962). It generally contains irregularly shaped anhedral to subhedral quartz intergrowths forming a graphic texture (Fig. 7c). The plagioclase also contains small biotite inclusions. Biotite and sericite are also commonly found along the rim of the pre-existing K-feldspar megacryst (Figs 6a, 7a,b). A direct relation exists between the size of the core and the size of the orbicule. The main axis of the core is always parallel to the main axis of the orbicule. The core generally occupies around 20 to 40 % (30 % on average) of the width of the orbicule and between 35 and 60 % (50 % on average) of its length. The cores are rarely formed by two adjacent megacrysts, which produces orbicules with irregular shapes (Fig. 6a).

The inner shell surrounds the core and consists of radial and equant plagioclase crystals (Figs 6a, 7). The radial crystals radiate from the edges of the core outwards, increasing in width in this direction. Both types of crystals contain scarce inclusions of biotite, positioned either randomly or concentrically, and of quartz. The inner shell commonly occupies between 20 and 35 % (25 % on average) of the width of the orbicule.

The inner shell is interrupted by a thin, 0.2 to 3 mm thick, dark layer. This layer consists of tangentially oriented biotite laths (Figs 6a, 7). The biotite crystals have sizes between 0.2 and 2.5 mm and straw-coloured to dark brown pleochroism. They contain abundant inclusions of small, anhedral apatite; inclusions of zircon are also found. Muscovite is present as thin laths in contact with the biotite crystals.

The outer shell consists of radial plagioclase crystals forming a distinctive plumose texture (Figs 6a, 7). The radial crystals can either originate after the dark layer

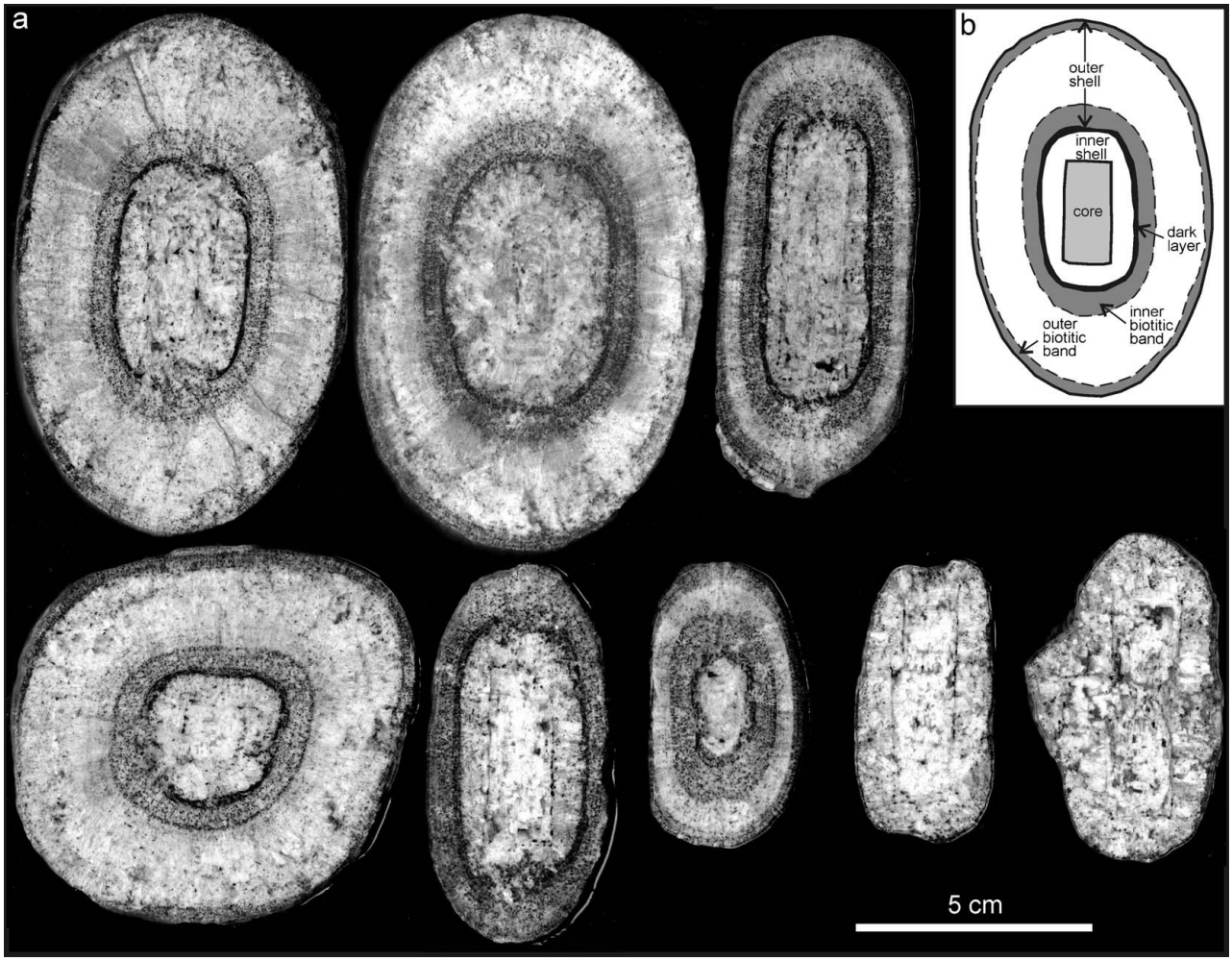

Figure 6. (a) Polished sections of orbicules from the Velasco orbicular granitoid. All sections are parallel to the main axis except the lower left which is perpendicular to the main axis. Note the irregular outline of the lower right orbicule caused by the presence of two megacrysts in the core. (b) Sketch showing the zones of an orbicule.

or be a continuation of radial crystals from the inner shell. Contacts between the radial crystals are irregular. Small elongated muscovite and quartz crystals are found along them. Around the inner part of this shell, an inner diffuse band is present, composed of tangentially oriented biotite laths forming diffuse rings (Figs 6a, 7). Similarly, an outer diffuse band is typically present around the outer part of the shell (Fig. 6a). Between both bands, the radial plagioclase also contains small biotite inclusions, but in much lower quantities. The outer shell generally occupies between 35 and 60 % (45 % on average) of the width of the orbicule.

The inter-orbicular matrix has a variable texture ranging from aplitic to pegmatitic, the latter being more common. The matrix is generally finer-grained close to the orbicules and its grain size increases towards the inter-orbicular spaces (Fig. 8). It consists of K-feldspar (45–50 %), quartz (25–35 %) and plagioclase (20–25 %), with biotite, muscovite and scarce apatite as accessory minerals (Fig. 8). The mica abundance is quite variable, generally between 3 and 10 %.

A small, 2 × 1 m, pegmatite pod is present in the orbicular body (Fig. 2). This pegmatite consists of large pink K-feldspar, quartz and muscovite, and can be considered a final facies of the inter-orbicular matrix.

4. Whole-rock geochemistry

Whole-rock geochemistry was determined at the universities of Oviedo (major elements) and Huelva (trace elements), Spain. Major elements were analysed by X-ray fluorescence (XRF) with a Phillips PW2404 system, with a precision generally better than ± 1.5 % relative. Trace elements were analysed by inductively coupled plasma mass spectrometry (ICP-MS) with an HP-4500 system, with a precision for most elements between 5 and 10 % relative. Details on the method can be found in de la Rosa *et al.* (2001).

Six whole-rock chemical analyses of the orbicular granitoid and the surrounding rocks were carried out (Table 2). The analysed samples consist of two orbicules, two inter-orbicular matrix samples, one sample of the megacryst-rich Huaco granite in contact with the orbicular granitoid, and one sample of an aplite dyke also in contact with the orbicular granitoid. Table 2 also shows an estimate of the total composition of

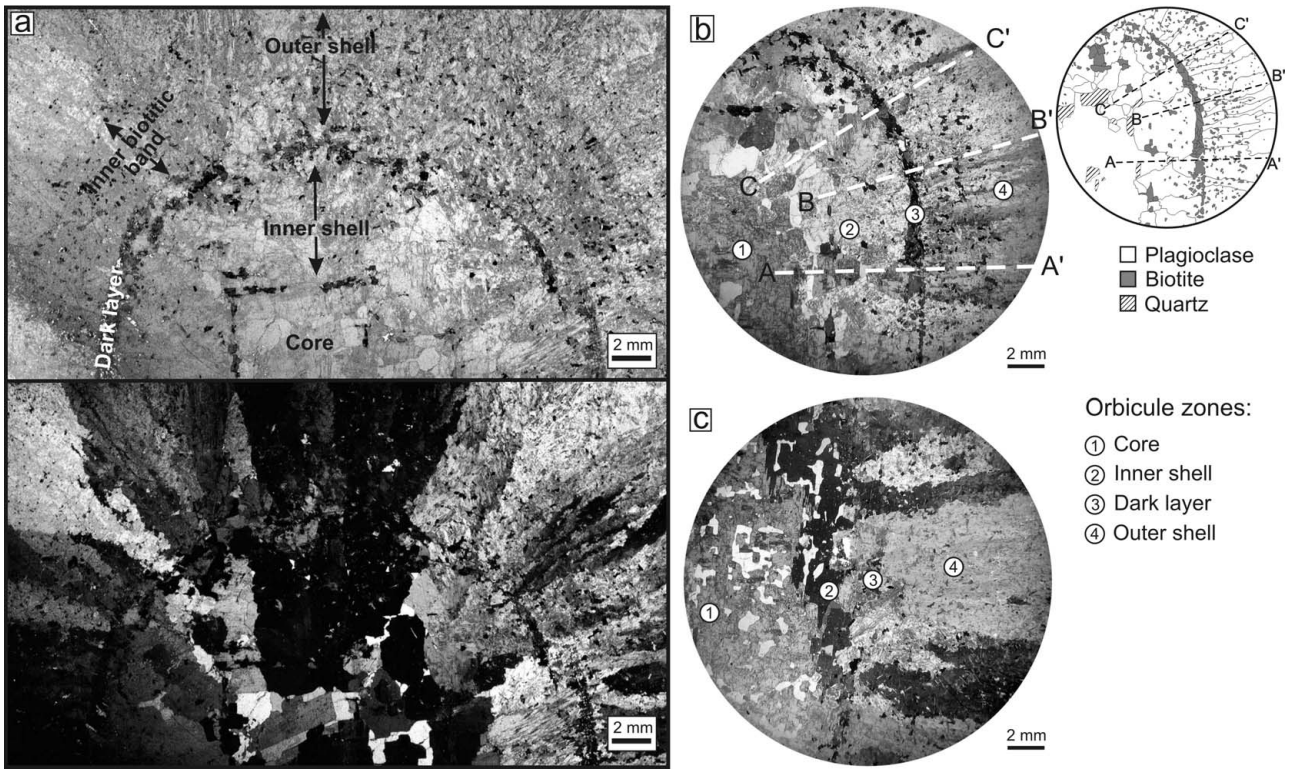

Figure 7. Scanned images of thin-sections of orbicules. (a) Thin-section under parallel light (top; zones are indicated) and crossed polars (bottom). (b) Thin-section under crossed polars showing the analysed microprobe profiles (see Fig. 10), and corresponding sketch showing the mineralogy. (c) Thin-section under crossed polars. Numbers in (b) and (c) indicate orbicules zones.

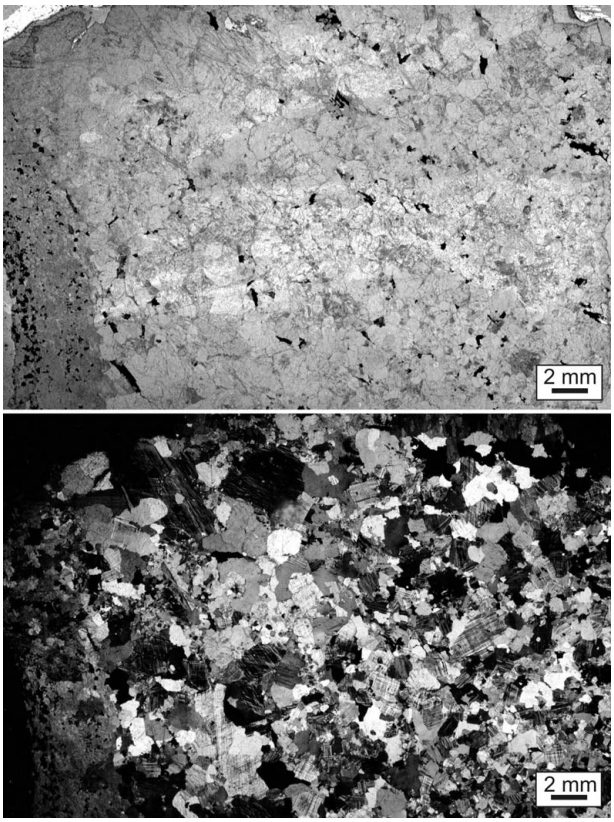

Figure 8. Scanned images of a thin-section of the inter-orbicular matrix under parallel (top) and crossed polars (bottom). Toward the left, the matrix was in contact with an orbicule; note grain-size increase toward the centre of the thin-section.

the orbicular granitoid (orbicules + matrix) calculated considering a proportion of 58 % orbicules and 42 % matrix. Also included in Table 2 is the average composition of the Huaco granite calculated from 11 analyses (taken from Grosse *et al.* 2009). The chemical data are shown in normalized variation diagrams (Fig. 9).

The two analysed orbicules are chemically similar. Both are poor in SiO_2 and K_2O and very rich in Al_2O_3, CaO and Na_2O (Fig. 9a) compared to the Huaco granite, consistent with plagioclase being the main mineral phase of the orbicules. The ferromagnesian and P_2O_5 contents of the orbicules are slightly lower than in the Huaco granite (Fig. 9a). The orbicules are leucocratic and moderately peraluminous. The inter-orbicular matrix has a composition similar to the Huaco granite in terms of SiO_2, Al_2O_3, CaO, Na_2O, K_2O and P_2O_5 (Fig. 9a). On the other hand, the matrix has a lower ferromagnesian content than the Huaco granite (Fig. 9a). Considering both orbicules and matrix, the estimated orbicular granitoid composition has lower SiO_2, K_2O and ferromagnesian contents and higher Al_2O_3, CaO and Na_2O contents compared to the Huaco granite (Fig. 9a). The megacryst-rich Huaco granite in contact with the orbicular granitoid is characterized by high Al_2O_3, Na_2O and K_2O concentrations and low ferromagnesian contents (Fig. 9a), consistent with K-feldspar abundance and lack of mafic minerals. The aplite in contact with the orbicular granitoid is rich in SiO_2 and alkalis and poor in CaO and ferromagnesian oxides.

Table 2. Whole-rock chemical analyses of the Velasco Orbicular Granitoid

	Orbicular granitoid							
	Orbicules		Matrix		Total*	Megacryst-rich Huaco granite†	Aplite	HG mean§
Sample	6764	7743O	6765	7743M	(calc.)	7748	7753	(n = 11)
Major oxides (wt%)								
SiO_2	62.43	61.92	73.04	73.47	66.83	69.51	73.08	73.08
TiO_2	0.19	0.16	0.14	0.16	0.16	0.06	0.12	0.25
Al_2O_3	21.75	21.82	13.88	13.89	18.47	16.88	14.43	13.64
$Fe_2O_3^{tot}$	1.81	1.81	1.38	2.01	1.76	0.64	1.34	2.27
MgO	0.29	0.21	0.20	0.23	0.23	0.00	0.00	0.32
MnO	0.05	0.06	0.04	0.06	0.05	0.02	0.03	0.05
CaO	2.98	3.29	0.71	0.89	2.15	0.46	0.68	0.83
Na_2O	8.18	8.61	2.88	2.91	6.09	3.81	3.38	3.04
K_2O	1.22	0.95	6.20	5.50	3.08	8.11	6.33	5.20
P_2O_5	0.19	0.18	0.22	0.24	0.20	0.16	0.15	0.24
P.F.	1.05	0.67	0.63	0.60	0.76	0.45	0.40	0.69
Total	100.14	99.67	99.31	99.96	99.79	100.11	99.92	99.62
A/(CNK)	1.08	1.03	1.09	1.13	1.08	1.06	1.06	1.13
Trace elements (ppm)								
Li	233	182	164	189	194	81	–	172
Be	27	28	13	14	22	12	–	14
Sc	3.8	3.0	2.7	4.8	3.6	1.2	–	5.3
V	14	10	9.2	7.5	10	2.9	–	15
Cr	78	8.2	35	17	36	5.8	–	70
Co	67	14	28	21	34	16	–	32
Ni	15	7.8	7.8	11	11	7.1	–	20
Zn	48	68	38	67	56	25	–	68
Ga	45	39	34	31	38	32	–	32
Rb	157	125	360	317	224	476	–	312
Sr	156	121	83	42	107	79	–	53
Y	16	17	18	31	20	10	–	26
Zr	24	14	25	57	28	23	–	107
Nb	26	25	27	45	30	12	–	36
Cs	30	22	40	33	30	23	–	34
Ba	91	41	222	118	110	388	–	192
La	33	27	17	18	25	11	–	33
Ce	62	53	36	43	50	20	–	71
Pr	7.0	6.4	4.0	5.5	5.9	2.5	–	9.3
Nd	30	22	18	20	23	9	–	38
Sm	6.5	4.8	4.2	5.1	5.2	1.9	–	8.1
Eu	2.1	1.7	1.0	0.76	1.5	1.3	–	0.76
Gd	5.2	4.3	3.8	5.0	4.6	1.8	–	7.0
Tb	0.69	0.75	0.60	1.0	0.76	0.34	–	1.1
Dy	4.2	3.9	4.1	6.1	4.5	1.9	–	5.9
Ho	0.55	0.68	0.61	1.2	0.74	0.37	–	1.0
Er	1.4	1.5	1.8	3.3	1.9	1.0	–	2.5
Tm	–	0.21	0.16	0.57	0.23	0.15	–	0.29
Yb	0.9	1.2	1.7	3.5	1.7	0.9	–	2.1
Lu	–	0.16	0.11	0.54	0.19	0.14	–	0.24
Ta	14	3.8	12	8.2	9.4	3.4	–	8.9
Pb	32	30	41	33	34	48	–	31
Th	19	17	13	19	17	6.9	–	28
U	5.1	7.9	6.1	8.4	6.8	3.7	–	7.9

*Calculated composition of the orbicular granitoid considering 58% orbicules and 42% matrix.
†Megacryst-rich Huaco granite in contact with the orbicular granitoid.
§Average composition of the Huaco granite calculated from 11 analyses from Grosse *et al.* (2009).

The orbicules have high Sr and Eu contents, consistent with plagioclase abundance, and low Rb and Ba contents, consistent with K-feldspar scarcity (Fig. 9b). Most transition element contents are lower than in the Huaco granite, whereas Li, Be and Ga contents are higher (Fig. 9b). The trace element concentrations of the two analysed inter-orbicular matrix samples are quite variable. In comparison with the Huaco granite, both samples are poor in transition elements, Th and the LREE, whereas one sample is enriched in Cs, Rb, Sr, Ba, Ta and Pb, and the other in Nb, Y and the HREE (Fig. 9b). Trace element contents in the megacryst-rich Huaco granite are generally low, except for Rb, Ba and Pb (Fig. 9b), which are commonly concentrated in K-feldspar.

In a chondrite-normalized REE diagram (Fig. 9c), the orbicules have profiles with strongly decreasing slopes ($(La/Yb)_N$ = 15.4 and 24.3), suggesting LREE enrichments, and slightly positive Eu anomalies (Eu/Eu^* = 1.09 and 1.15), in agreement with the elevated plagioclase content. The inter-orbicular matrix samples have less steep negative slopes than the Huaco granite ($(La/Yb)_N$ = 3.5 and 6.5). They show negative Eu anomalies (Eu/Eu^* = 0.47 and 0.78), indicative of

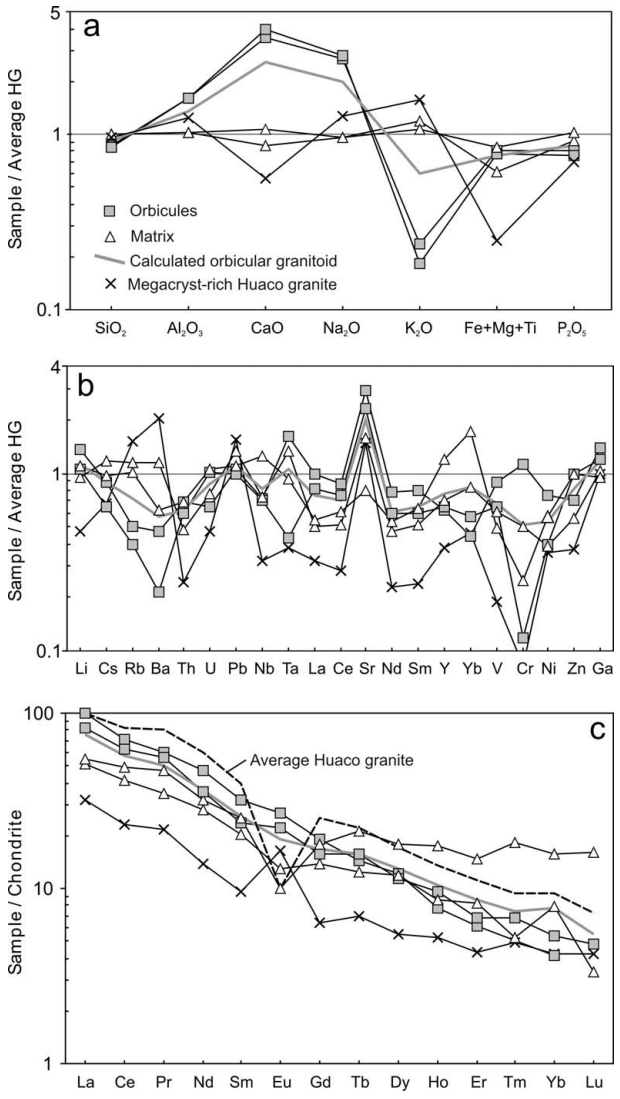

Figure 9. Normalized geochemical variation diagrams of the Velasco orbicular granitoid. (a) Major oxides normalized to the average Huaco granite. (b) Trace elements normalized to the average Huaco granite. (c) REE normalized to chondrite of Nakamura (1974).

plagioclase fractionation. The megacryst-rich Huaco granite has a moderately decreasing slope ($(La/Yb)_N = 7.5$) and a strong positive Eu anomaly ($Eu/Eu^* = 2.12$), compatible with Eu concentration in the K-feldspar megacrysts.

5. Mineral chemistry

Chemical analyses of minerals were carried out using a Cameca SX-50 microprobe at the Institut für Mineralogie, Petrologie und Geochimie, Ludwig-Maximilians-Universität, Munich, Germany. Measurement conditions were a beam current intensity of 20 nA and an acceleration voltage of 15 keV.

K-feldspar, plagioclase and biotite from two orbicules (Fig. 7b, c) and from one inter-orbicular matrix sample were analysed. The mineral structural formulas were calculated based on 32 (feldspars) and 22 oxygens (biotite). Tables 3, 4 and 5 show the obtained results.

Table 3. Chemical composition (in wt%) and structural formula of selected plagioclase points along three profiles of an orbicule (see Figs 7b, 10)

	Core crystal A					Plumose crystal A (inner-outer shell)				Plumose crystal B (inner shell)					Plumose crystal B (outer shell)					Plumose crystal C (outer shell)				
D (mm)	0.00	0.85	1.62	2.30	2.98	3.15	4.26	5.79	7.07	8.34	0.15	0.87	1.60	2.32	2.98	3.41	4.14	5.23	6.17	7.04	4.22	5.25	6.55	7.32	8.27
Sample	P1–100	P1–90	P1–81	P1–73	P1–65	P1–63	P1–50	P1–32	P1–17	P1–02	P2–96	P2–86	P2–76	P2–66	P2–57	P2–51	P2–41	P2–26	P2–13	P2–01	P3–51	P3–39	P3–24	P3–15	P3–04
SiO_2	64.02	65.03	65.30	65.51	66.15	68.35	66.12	63.96	64.73	64.83	66.84	65.43	65.25	64.84	64.52	65.34	65.83	65.94	63.41	65.05	66.56	65.84	65.05	63.91	65.21
Al_2O_3	21.46	21.40	21.47	20.47	19.78	20.43	21.46	21.75	21.59	21.52	21.87	23.57	22.66	22.51	22.14	21.97	21.59	21.09	21.87	21.58	20.76	20.92	22.22	22.87	22.54
CaO	3.65	3.39	3.29	2.65	1.91	2.05	2.50	4.04	3.37	3.70	2.65	3.52	3.05	4.00	4.24	3.78	3.11	2.88	4.02	3.75	2.68	2.91	3.62	3.93	4.11
Na_2O	9.44	9.93	9.62	10.09	10.68	10.85	9.94	9.58	9.97	9.68	10.07	9.00	9.30	9.18	9.23	9.74	9.77	10.18	9.39	9.46	10.41	10.13	9.69	9.52	9.26
K_2O	0.17	0.11	0.17	0.20	0.07	0.08	0.11	0.11	0.09	0.10	0.13	0.25	0.12	0.09	0.09	0.10	0.15	0.11	0.09	0.14	0.13	0.16	0.09	0.09	0.17
FeO*	0.00	0.03	0.04	0.00	0.03	0.02	0.49	0.02	0.04	0.00	0.00	0.05	0.05	0.02	0.00	0.28	0.13	0.00	0.00	0.06	0.03	0.39	0.01	0.09	0.03
Total	98.94	100.01	99.93	99.18	98.89	101.90	100.82	99.55	99.92	99.97	101.65	101.98	100.55	100.79	100.34	101.43	100.67	100.45	98.87	100.14	100.69	100.55	100.80	100.46	101.43
Si	11.43	11.48	11.51	11.65	11.78	11.78	11.56	11.36	11.44	11.45	11.56	11.30	11.41	11.35	11.36	11.40	11.52	11.58	11.33	11.46	11.64	11.57	11.39	11.25	11.35
Al	4.52	4.45	4.46	4.29	4.15	4.15	4.42	4.56	4.50	4.48	4.45	4.80	4.67	4.64	4.59	4.52	4.45	4.36	4.61	4.48	4.28	4.33	4.58	4.74	4.62
Ca	0.70	0.64	0.62	0.50	0.36	0.38	0.47	0.77	0.64	0.70	0.49	0.65	0.57	0.75	0.80	0.71	0.58	0.54	0.77	0.71	0.50	0.55	0.68	0.74	0.77
Na	3.27	3.40	3.29	3.48	3.68	3.62	3.37	3.30	3.42	3.32	3.38	3.01	3.15	3.12	3.15	3.30	3.32	3.47	3.25	3.23	3.53	3.45	3.29	3.25	3.13
K	0.04	0.02	0.04	0.05	0.02	0.02	0.03	0.02	0.02	0.02	0.03	0.06	0.03	0.02	0.02	0.02	0.03	0.02	0.02	0.03	0.03	0.04	0.02	0.02	0.04
An	17.42	15.77	15.72	12.54	8.95	9.42	12.10	18.79	15.68	17.33	12.60	17.51	15.25	19.29	20.15	17.56	14.84	13.43	19.05	17.84	12.39	13.57	17.03	18.49	19.52
Ab	81.59	83.64	83.31	86.33	90.63	90.14	87.24	80.61	83.83	82.12	86.68	81.01	84.04	80.21	79.32	81.86	84.29	85.98	80.44	81.37	86.91	85.55	82.49	81.01	79.54
Or	0.99	0.59	0.97	1.13	0.42	0.44	0.66	0.60	0.49	0.55	0.71	1.48	0.72	0.49	0.53	0.58	0.87	0.59	0.51	0.79	0.70	0.88	0.48	0.50	0.94

Structural formulas calculated based on 32 oxygens; *D* is the distance in mm along the profile; *Total Fe calculated as FeO.

Table 4. Chemical composition (in weight %) and structural formula of K-feldspar and plagioclase from the inter-orbicular matrix and average compositions of these minerals in the Huaco granite

	Inter-orbicular matrix										
	K-feldspar					Plagioclase				Huaco granite	
Sample	M-02-fk	M-10-fk	M-11-fk	M-15-fk	M-20-fk	M-06-pl	M-16-pl	M-17-pl	M-18-pl	K-feld. avg.	Plag avg.
SiO_2	65.31	66.39	66.41	66.05	65.92	64.43	65.33	65.07	67.52	65.34	64.68
Al_2O_3	18.31	18.48	18.67	18.76	18.44	22.13	22.03	22.39	21.88	18.24	22.35
CaO	0.00	0.00	0.00	0.00	0.00	3.68	3.49	3.94	2.64	0.00	3.83
Na_2O	0.70	1.39	1.22	1.38	1.03	9.84	9.69	9.31	10.09	0.85	9.58
K_2O	15.95	14.70	14.91	15.23	15.59	0.21	0.14	0.15	0.06	15.55	0.05
FeO*	0.02	0.06	0.02	0.03	0.01	0.00	0.00	0.04	0.01	0.03	0.02
Total	100.42	101.02	101.23	101.45	100.98	100.30	100.70	100.91	102.20	100.01	100.52
Si	12.02	12.06	12.04	11.99	12.03	11.35	11.43	11.37	11.59	12.04	11.35
Al	3.97	3.96	3.99	4.01	3.96	4.60	4.54	4.61	4.43	3.96	4.62
Ca	0.00	0.00	0.00	0.00	0.00	0.69	0.65	0.74	0.49	0.00	0.72
Na	0.25	0.49	0.43	0.49	0.36	3.36	3.29	3.16	3.36	0.30	3.26
K	3.74	3.41	3.45	3.52	3.63	0.05	0.03	0.03	0.01	3.66	0.01
An	0.00	0.00	0.00	0.00	0.00	16.92	16.45	18.78	12.58	0.00	18.05
Ab	6.25	12.54	11.08	12.10	9.13	81.94	82.74	80.35	87.10	7.63	81.67
Or	93.75	87.46	88.91	87.89	90.87	1.14	0.81	0.87	0.32	92.37	0.28

Structural formulas calculated based on 32 oxygens; *Total Fe calculated as FeO.

Table 5. Chemical composition (in wt %) and structural formula of representative biotite crystals from orbicules and the inter-orbicular matrix, and average composition of biotite from the Huaco granite (HG)

	Orbicule														
Zone	Core		Inner shell		Dark layer					Outer shell		Inter-orbicular matrix			
Sample	2–71	3–80	2–28	2–37	3	4–01	4–07	5	6–06	b-17	b-22	M-01	M-04	M-09	avg.
SiO_2	35.18	35.02	34.90	34.50	34.21	35.46	37.22	34.98	34.62	35.65	34.36	35.15	33.89	34.29	33.85
TiO_2	2.44	2.66	2.53	2.25	2.38	2.46	2.48	2.35	2.10	2.34	2.39	1.98	2.44	2.20	2.73
Al_2O_3	18.22	18.30	17.99	16.93	18.76	18.06	18.90	17.15	17.47	16.87	17.36	18.21	17.69	18.10	17.16
FeO*	26.04	26.63	26.72	26.95	25.97	26.28	24.00	26.33	26.21	24.81	25.89	25.86	26.79	26.13	26.39
MnO	0.93	0.66	0.89	0.86	0.90	0.82	0.78	0.77	0.68	0.81	0.68	1.01	0.73	0.79	0.44
MgO	3.22	3.20	3.00	2.92	3.04	3.24	3.14	3.40	3.11	3.05	2.65	2.85	2.64	2.72	3.93
CaO	0.06	0.00	0.01	0.02	0.03	0.03	0.16	0.15	0.04	0.00	0.00	0.00	0.00	0.00	0.00
Na_2O	0.05	0.09	0.09	0.08	0.03	0.07	0.11	0.10	0.04	0.02	0.06	0.08	0.07	0.11	0.09
K_2O	8.57	8.79	8.69	8.25	8.95	8.78	8.10	8.70	8.58	9.10	9.44	9.36	9.38	9.50	9.36
$Li_2O^{\dagger}$	0.50	0.50	0.54	0.55	0.53	0.50	0.51	0.47	0.52	0.53	0.61	0.57	0.61	0.59	0.40
$H_2O^{\S}$	3.82	3.83	3.81	3.72	3.79	3.84	3.91	3.77	3.73	3.75	3.72	3.80	3.73	3.76	3.74
Total	99.03	99.68	99.17	97.04	98.58	99.52	99.30	98.17	97.09	96.92	97.16	98.86	97.98	98.19	98.11
Si	5.52	5.48	5.50	5.56	5.41	5.54	5.71	5.56	5.56	5.70	5.54	5.55	5.44	5.47	5.42
Al^{IV}	2.48	2.52	2.50	2.44	2.59	2.46	2.29	2.44	2.44	2.30	2.46	2.45	2.56	2.53	2.58
Al^{VI}	0.89	0.85	0.83	0.78	0.91	0.87	1.12	0.78	0.87	0.89	0.84	0.93	0.79	0.88	0.66
Ti	0.29	0.31	0.30	0.27	0.28	0.29	0.29	0.28	0.25	0.28	0.29	0.24	0.29	0.26	0.33
Fe^{2+}	3.42	3.48	3.52	3.63	3.44	3.44	3.08	3.50	3.52	3.32	3.49	3.41	3.60	3.49	3.54
Mn	0.12	0.09	0.12	0.12	0.12	0.11	0.10	0.10	0.09	0.11	0.09	0.13	0.10	0.11	0.06
Mg	0.75	0.74	0.70	0.70	0.72	0.75	0.72	0.81	0.74	0.73	0.64	0.67	0.63	0.65	0.94
Li*	0.32	0.32	0.34	0.36	0.34	0.31	0.32	0.30	0.33	0.34	0.40	0.36	0.40	0.38	0.26
Ca	0.01	0.00	0.00	0.00	0.00	0.01	0.03	0.03	0.01	0.00	0.00	0.00	0.00	0.00	0.00
Na	0.02	0.03	0.03	0.03	0.01	0.02	0.03	0.03	0.01	0.01	0.02	0.02	0.02	0.03	0.03
K	1.72	1.75	1.74	1.70	1.81	1.75	1.58	1.76	1.76	1.86	1.94	1.88	1.92	1.93	1.91
#Fe	0.82	0.82	0.83	0.84	0.83	0.82	0.81	0.81	0.83	0.82	0.85	0.84	0.85	0.84	0.79

Structural formulas calculated based on 22 oxygens; *Total Fe calculated as FeO; $^{\dagger}Li_2O$ calculated with equation (1) of Tischendorf, Förster & Gottesmann (1999); $^{\S}H_2O$ calculated assuming that the (F, Cl, OH) site is full; #Fe = Fe/(Fe+Mg).

Also shown in these tables are the average compositions of K-feldspar, plagioclase and biotite of the Huaco granite (taken from Grosse *et al.* 2006).

5.a. Plagioclase from orbicules

The chemical composition of plagioclase was determined along three profiles through an orbicule sample (Table 3; Figs 7b, 10). Profile A comprises an equant core crystal and a plumose crystal that spans the inner and outer shells (Fig. 10a). Profile B covers a thick plumose crystal from the inner shell and a thin plumose crystal from the outer shell (Fig. 10b). Profile C comprises several equant crystals from the inner shell and a plumose crystal from the outer shell (Fig. 10c).

The equant core crystal shows a statistically significant normal chemical zonation trend ($P < 0.005$; 99.5 % confidence level) of decreasing anorthite content from $\sim An_{20}$ at the centre to $\sim An_{10}$ at the edge of the crystal (Fig. 10a). The five small equant crystals of the inner

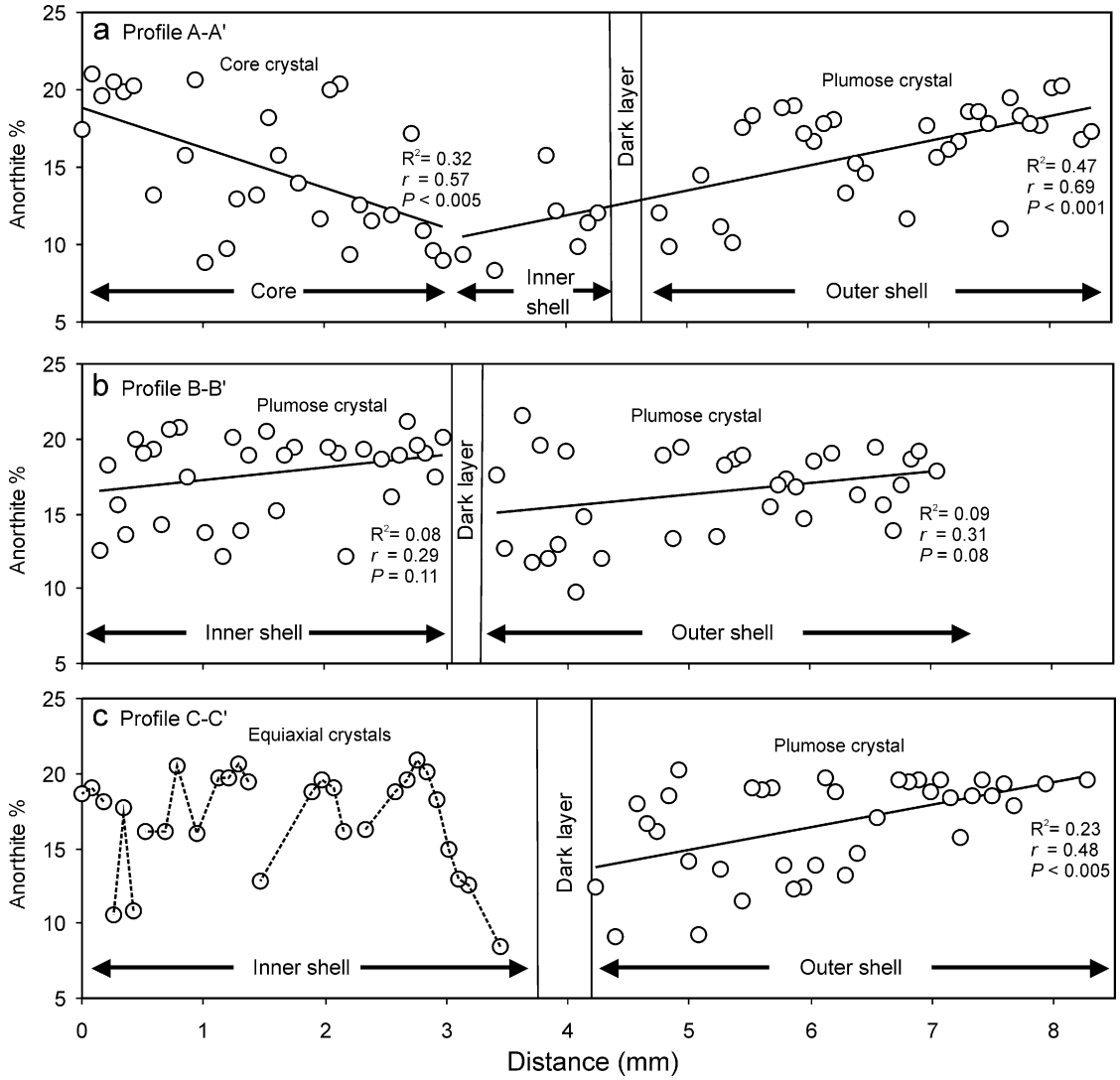

Figure 10. Diagrams showing the variations in anorthite content of plagioclase along three profiles through an orbicule (see Fig. 7b). Straight lines are calculated linear regressions through the data points of five large crystals; R^2 is the coefficient of determination; *r* is the correlation coefficient; *P* is the significance level of the linear trend. In profile C–C′, dotted lines connect the data points of five small equant crystals.

shell have variable compositions between An_9 and An_{21} (Fig. 10c). The profile along three of these crystals suggests normal chemical zonations of decreasing anorthite content from centre to edges (Fig. 10c), although the limited number of points along each crystal prevents a statistical analysis.

In contrast, the four plumose crystals, both from the inner and outer shells, show reverse chemical zoning trends of increasing anorthite content outwards, along the growth direction (Fig. 10). Although the scatter of points is quite large on all four plumose crystals (low R^2 values, Fig. 10), linear regression analyses indicate that two of the trends are statistically significant at $P < 0.005$, whereas the other two trends are significant at $P \sim 0.1$ (~ 90 % confidence level) (Fig. 10). In general, the anorthite concentration of the plumose crystals increases from $\sim An_{10–15}$ to $\sim An_{20}$, along the growth directions, spanning distances of 3 to 5 mm (Fig. 10).

5.b. K-feldspar and plagioclase from the inter-orbicular matrix

The matrix K-feldspar composition (Table 4) is $Or_{87–94}$, similar to the K-feldspar of the Huaco granite ($Or_{88–96}$). The matrix plagioclase (Table 4) is oligoclase ($An_{13–19}$), similar to the orbicular plagioclase and somewhat more albitic than the plagioclase of the Huaco granite ($An_{13–23}$).

5.c. Biotite

All of the orbicular and matrix biotite (Table 5) can be classified as biotite *s.s.* according to the classification of Deer, Howie & Zussman (1962) (Fig. 11) and as siderophyllite following the classification of Tischendorf *et al.* (1997). The chemical compositions of the orbicular biotite are in general intermediate

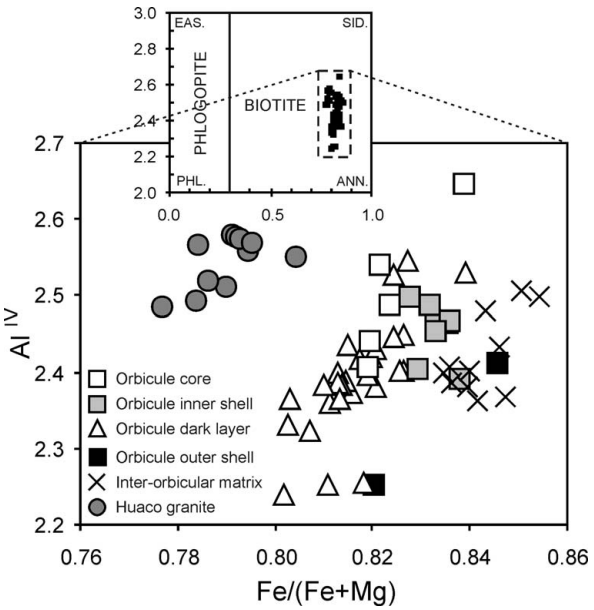

Figure 11. Al^{IV} v. Fe/(Fe+Mg) diagram (Deer, Howie & Zussman, 1962) of biotites from orbicules, the inter-orbicular matrix and the Huaco granite (taken from Grosse *et al.* 2006). EAS. – Eastonite; SID. – Siderophyllite; ANN. – Annite; PHL. – Phlogopite.

between the biotite of the Huaco granite and the biotite of the inter-orbicular matrix, being more similar to the latter (Fig. 11). Al and Mn contents increase and Ti and Mg contents decrease from the Huaco granite biotite toward the matrix biotite. The Fe/(Fe+Mg) ratio of the orbicular biotite is also intermediate, generally between 0.80 and 0.84, while the matrix biotite has higher Fe/(Fe+Mg) ratios between 0.83 and 0.85 (Fig. 11). Biotite crystals from the different orbicular zones do not show significant compositional differences.

6. Discussion

The orbicular granitoid of the Sierra de Velasco has exceptional petrological and geochemical characteristics that imply special conditions and processes of formation. In the following sections, we discuss different aspects of the formation of the orbicular granitoid.

6.a. A pocket of 'orbicular melt' within the Huaco granite

Field and petrographical observations suggest that the orbicular granitoid formed *in situ* in a pocket of 'orbicular melt' located within the Huaco granite: (1) irregular instead of dyke- or sheet-like shape of the orbicular body; (2) lack of evidence of mechanical transport of the orbicules, such as deformed or broken orbicules; (3) lack of progressive orbicule size and abundance variations within the orbicular granitoid that would be consistent with sorting or sedimentation processes; (4) the Huaco granite in contact with the orbicular granitoid shows an unusual increase in the abundance of K-feldspar megacrysts and contains scattered orbicules, suggesting that it was affected by the orbicular forming processes and not simply intruded by the 'orbicular melt'. Moreover, the irregular shape of the orbicular granitoid, its sinuous, even 'cauliflower-like' (e.g. Decitre, Gasquet & Marignac, 2002), contact with the Huaco granite, and the presence of scattered orbicules within the Huaco granite suggest that the granite was only partially crystallized when the pocket of 'orbicular magma' formed.

The site where the pocket of 'orbicular melt' developed within the Huaco granite is uncertain. The majority of orbicular rocks described in the literature are located near the margins or the roof of the enclosing igneous bodies. In these areas, water-rich melt fractions tend to segregate and collect in pockets or cupolas, a situation favourable for the formation of orbicular rocks (e.g. Moore & Lockwood, 1973; Ort, 1992). The Velasco orbicular granitoid is located far from the present margins of the Huaco granite (Fig. 1). It could be located close to the roof of the granite body, but the existing data neither support nor rule out this possibility. Alternatively, the pocket of 'orbicular melt' could have developed within the Huaco magma chamber at a mostly-molten/mostly-solid boundary, that is, at a solidification front (Marsh, 1996).

If the pocket of 'orbicular melt' formed *in situ* within the partially crystallized Huaco magma, then it is likely that the 'orbicular melt' derived directly from the surrounding Huaco magma by some kind of melt extraction process. A valuable clue can be found by considering the K-feldspar megacryst abundances in the different studied rocks. The typical megacryst abundance in the Huaco granite is 30–35 %, whereas in the granite surrounding the orbicular granitoid the abundance is generally much higher. On the contrary, if the orbicular cores originally consisted of K-feldspar megacrysts (see Section 6.b), and if it is estimated that cores account for ~10 % of orbicule volumes (considering that, on average, cores occupy between 30 and 50 % of the axis of the orbicules), then an estimation of the abundance of megacrysts originally in the 'orbicular melt' would be ~6 % (considering that the average abundance of orbicules in the orbicular granitoid is 58 %). These different megacryst abundances suggest that some kind of process favoured the accumulation of megacrysts on the walls of the pocket of 'orbicular melt', with only a minority being incorporated in the melt itself. If it is assumed that the K-feldspar megacrysts crystallized relatively early (e.g. Vernon & Paterson, 2008), then the different megacryst abundances, and consequently the formation of the pocket, can be related to a mechanism of crystal–melt segregation by filter pressing (e.g. Propach, 1976). Several types of filter pressing mechanisms have been postulated, such as compaction (Bea *et al.* 1994; Bachmann & Bergantz, 2004), solidification front instabilities resulting from gravitational instabilities in the crystal mush (Marsh, 1996) and gas-driven filter pressing (Sisson & Bacon, 1999). Any of these mechanisms acting on the Huaco magma could have

resulted in the segregation of the interstitial melt (together with relatively few megacrysts and early-formed crystals) out of the crystal mush and into a newly formed pocket, leaving behind a concentration of megacrysts around this pocket.

Generation of the 'orbicular melt' by segregation of the interstitial melt of the surrounding Huaco magma implies that the 'orbicular melt' should have been initially evolved and volatile-rich. Textural and chemical characteristics of the orbicular granitoid are in agreement with derivation from an evolved and volatile-rich melt: mostly pegmatitic inter-orbicular matrix, presence of the pegmatite pod, abundant aplites in the vicinity, low ferromagnesian and high alumina and alkali contents, biotites with high Fe/(Fe+Mg) ratios. However, compared to the Huaco granite, the calculated total composition of the orbicular granitoid is poor in silica and potassium, and rich in calcium and sodium (Table 2), all of which do not seem compatible with derivation from an evolved interstitial melt of the Huaco magma. This discrepancy can be explained if it is considered that the calculated total composition of the orbicular granitoid does not take into account possible final silica- and potassium-rich melts that could be represented by the pegmatite pod within the orbicular granitoid and by the abundant aplites that crop out close to or in contact with the orbicular granitoid. Furthermore, the accumulation of K-feldspar megacrysts around the orbicular granitoid implies an initial impoverishment in megacrysts, and thus in potassium, of the 'orbicular melt'. Participation of an allochthonous, more mafic magma that modified the composition of the 'orbicular melt' does not seem viable since no evidence of a mafic component has been found.

6.b. The orbicule cores: megacrysts as nucleation seeds

The formation of orbicular structures implies crystal growth around solid cores that acted as nucleation centres (e.g. Vernon, 1985). In the Velasco orbicular granitoid, the cores consist of K-feldspar megacrysts, partially to totally replaced by plagioclase. The K-feldspar megacrysts probably derived from the surrounding Huaco granite mush, as proposed already by Quartino & Villar Fabre (1962), given the abundance of K-feldspar megacrysts in the Huaco granite with similar size and shape as the orbicular cores. Replacement of K-feldspar by plagioclase in the megacrysts indicates conditions of plagioclase stability and K-feldspar instability in the melt. Quartino & Villar Fabre (1962) attributed this replacement to metasomatism by a sodium-rich pegmatitic melt. The 'orbicular melt' would have had a high Na_2O/K_2O ratio because of the accumulation of potassium in the megacryst cumulates around the pocket, thus possibly favouring a replacement process.

If the K-feldspar megacrysts were entrained with the interstitial melt from the Huaco magma to the pocket of 'orbicular melt', then crystals of other early crystallizing phases (e.g. biotite, plagioclase) should also have been entrained and incorporated in the 'orbicular melt'. However, orbicules grew only around megacrysts, implying that they were the only solids in the 'orbicular melt' when orbicular crystallization began, and all other minerals were somehow destroyed or resorbed. Vernon (1985) proposed that superheating is a crucial process in the formation of orbicular rocks since it is an effective way of destroying nuclei (shown experimentally by Lofgren, 1983), thus forcing nucleation to occur only on solid objects (that is, the megacrysts). According to Vernon (1985), mechanisms that can produce superheating of magma are the intrusion of a hotter and more mafic magma or the incorporation of water, which promotes higher degrees of melt depolymerization (e.g. Fenn, 1977; London, 1992) and lowers the liquidus temperature of the magma, thus causing an effective superheating. Both mechanisms have been postulated in specific studies of orbicular rocks, such as Decitre, Gasquet & Marignac (2002) (assimilation of mafic magma) and Ort (1992) and Lindh & Näsström (2006) (water addition). In the case of the Velasco orbicular granitoid, there is no evidence of participation of a mafic magma. Water-induced superheating is a more likely mechanism if it is considered that the 'orbicular melt' was segregated from the partially crystallized Huaco magma; it would have been a residual melt, which typically concentrates volatiles, as is the case of pegmatite-forming melts (e.g. London, 2005). Water-induced superheating could have thus lowered the liquidus of the 'orbicular melt' causing destruction of nuclei and resorbtion of small crystals (e.g. Ort, 1992; Lindh & Näsström, 2006), whereas the large K-feldspar megacrysts survived as solids.

6.c. Orbicular growth by undercooling of the melt

The orbicule structure of concentric shells with radial and tangential crystal habits and the reverse zoning of the plumose plagioclase are evidence of disequilibrium conditions during crystallization of the orbicules. The radial growth of plagioclase around the cores indicates heterogeneous nucleation on the surface of the pre-existing megacrysts due to a lack of dispersed nuclei (e.g. London, 1992). Orbicule growth contrasts with equilibrium crystallization typical of plutonic rocks, where nucleation is homogeneous and crystals have equant habits, form a non-oriented crystalline aggregate and are not zoned (e.g. Lofgren, 1974*a*; London, 1992).

Numerous experimental studies show that disequilibrium crystallization generating heterogeneous nucleation and radial habits can be obtained by rapid melt undercooling (e.g. Lofgren, 1974*a*; Lofgren & Donaldson, 1975; Fenn, 1977; Swanson, 1977; London, Morgan & Hervig, 1989; London, 1992). The reverse zoning of the plumose plagioclase crystals of the orbicules (anorthite content increases in the direction of crystal growth, Fig. 10) also suggests undercooling of the melt. Lofgren (1974*a*,*b*)

experimentally reproduced reverse zoning in plagioclase by rapid undercooling of a melt at isothermic conditions. This situation produces disequilibrium crystallization, reflected in reverse plagioclase zoning. Isothermal conditions during the crystallization of the plumose plagioclase is consistent with the similar compositions of biotite from the different orbicule zones. Durant & Fowler (2002) found the same type of reverse zoning in plagioclase and pyroxene in an orbicular diorite.

The destruction of nuclei caused by water concentration and superheating delays crystallization and induces significant undercooling (Vernon, 1985; London, 1992). Superheating followed by undercooling of the melt has been proposed as a key mechanism for the formation of orbicular rocks (e.g. Vernon, 1985; Ort, 1992; Lindh & Näsström, 2006). Undercooling of a melt can be accentuated by a sudden water pressure loss and exsolution of the volatile phase (e.g. Lofgren & Donaldson, 1975; Vernon, 1985; Hort, 1998), which raises the magma liquidus temperature. Water exsolution can occur as a consequence of different processes. One possibility is the rapid ascent of the melt, for example, as a dyke; however, the evidence for *in situ* formation of the orbicular granitoid rules out this mechanism. Two viable mechanisms that do not require transport of the 'orbicular melt' are: (1) water pressure release associated with a volcanic eruption, as proposed by Ort (1992); and (2) fracturing of a mostly-crystallized part of the wall-rock and consequent degassing of the 'orbicular melt'.

During orbicule crystallization, radial plagioclase grew continuously, while biotite crystallized sporadically, producing concentric layers and bands. This distribution of biotite in successive layers or rings suggests a crystallization ruled by fluctuations of biotite saturation in the melt. Each time biotite saturation was reached, biotite precipitated on the orbicule front producing the various layers. Crystallization during undercooling facilitates oscillatory or rhythmic supersaturation phenomena (e.g. McBirney & Noyes, 1979; Vernon, 1985) and compositional layering, as indicated, for example, by Lofgren & Donaldson (1975) for the formation of comb-layers, and by London (1992, 2005) for the formation of layered aplites.

Orbicular rocks are commonly associated with comb-layered rocks (e.g. Moore & Lockwood, 1973; Durant & Fowler, 2002). The plumose plagioclase of the orbicules is similar to comb-layer structures that, according to Lofgren & Donaldson (1975), Donaldson (1977) and London (1992), are formed by undercooling processes. Moore & Lockwood (1973) assert that comb-layer and orbicular growth are equivalent, with the difference that, in the former case, crystallization occurs on the walls of a magma chamber, whereas in the latter case, it occurs on dispersed solid seeds within the magma.

Orbicular growth also has some strong similarities to pegmatite crystallization. Pegmatite evolution involves disequilibrium crystallization from undercooled flux-bearing granitic melts, and heterogeneous nucleation, radial crystal growth, plumose habit and layering are all typical of pegmatites (e.g. London, 1992, 2005). However, an essential difference is that pegmatite melts seem to lack entrained crystals, implying that melt extraction from the magma body is very efficient and no crystals are entrained (London, 2005).

6.d. The crystallization of the inter-orbicular matrix

At a certain point, orbicule growth ceased and the inter-orbicular matrix crystallized. The normal and equant texture of the matrix implies a change in crystallization conditions from heterogeneous to homogeneous nucleation. This change was evidently abrupt, judging from the sharp contacts between orbicules and matrix, a common feature of orbicular rocks (e.g. Vernon, 1985). The two orbicule size populations suggest that the shift from orbicular to normal crystallization did not occur all at the same time, but rather during two stages with seemingly random distributions, probably dependent on local conditions; the first, less widespread shift occurred when the orbicules were still relatively small, and the second and main shift occurred when the orbicules had grown to larger, 'normal' sizes. As suggested by Vernon (1985), cooling of the 'orbicular melt' will eventually produce sufficient polymerization of the melt to generate dispersed nuclei causing the shift from orbicular to normal crystallization. The abruptness of the shift may reflect what experiments have shown as the quite sudden appearance of nuclei after a 'lag time' (e.g. Fenn, 1977; Swanson, 1977).

As discussed by Decitre, Gasquet & Marignac (2002) and Lindh & Näsström (2006), the shift from orbicular to normal crystallization is analogous to the solidification process of steel ingots in metallurgy, which show a shift from columnar (equivalent to the plumose plagioclase) to equiaxed (equivalent to the matrix) solidification. This columnar-to-equiaxed transition is evidently associated with melt polymerization and increase in nucleation density, since in industry, equiaxed growth is provoked by adding particles called 'refiners' that act as nucleation sites. A number of studies (e.g. Hunt, 1984; Siqueira, Cheung & Garcia, 2002; Martorano & Biscuola, 2009) indicate that the columnar-to-equiaxed transition in steel ingots occurs when the temperature gradient in the melt reaches a minimum critical value. Thus, the zones with smaller orbicules may have shifted to equiaxed crystallization earlier because in these zones the effective temperature of the melt decreased faster and reached a minimum critical value first.

The matrix size increment from the orbicule margins towards the inter-orbicular spaces suggests a crystallization in this direction, culminating with true pegmatites such as the small pegmatitic pod found within the orbicular body. Moreover, biotite compositions in the Huaco granite, the orbicules and the inter-orbicular matrix indicate conditions of progressive differentiation in this direction (e.g. Villaseca & Barbero, 1994; Fig. 11).

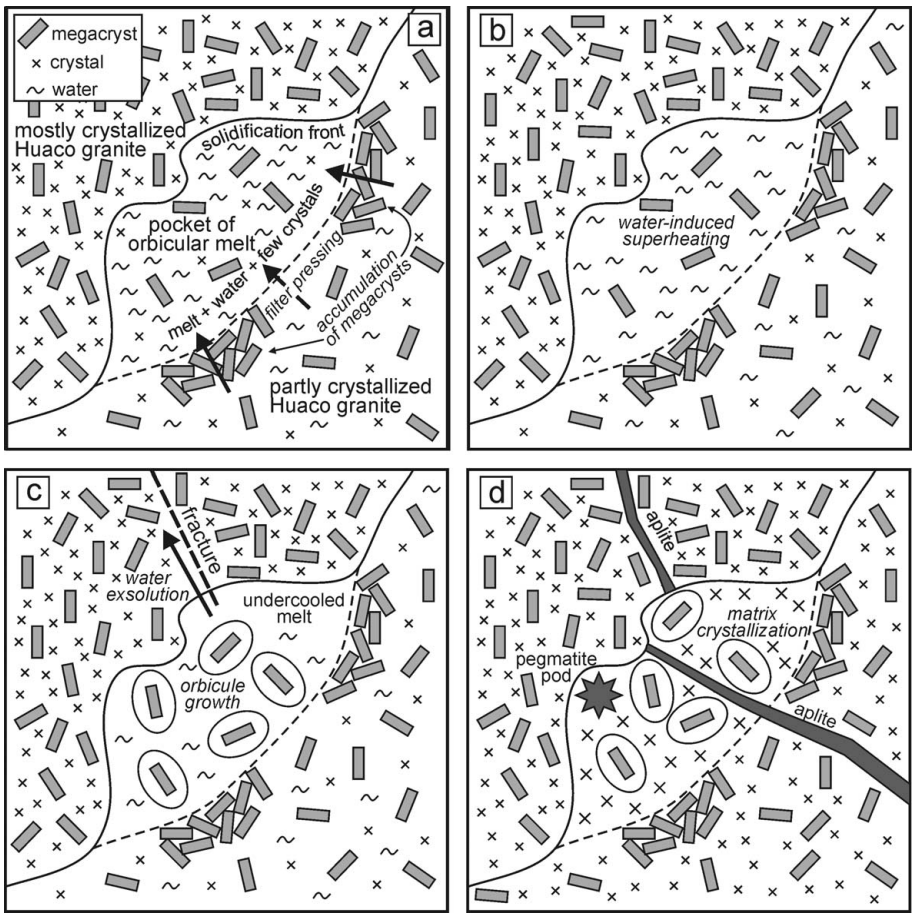

Figure 12. Cartoon of proposed genetic model for the Velasco orbicular granitoid. See text for explanations.

Final melts concentrated in silica and potassium may be represented by the pegmatite pod and the numerous aplite dykes and irregular bodies found around the orbicular granitoid.

7. Genetic model for the Velasco orbicular granitoid and implications for the origin of orbicular rocks

Based on the obtained data and the above considerations, we propose below a genetic model for the formation of the Velasco orbicular granitoid (Fig. 12). Our model is similar to the general model of Vernon (1985) for the formation of orbicular granitoids, as well as the specific model of Ort (1992).

(1) Formation of a pocket of 'orbicular melt' within the partially crystallized Huaco granite, possibly at a solidification front, by segregation of an evolved and volatile-rich melt via a filter-pressing mechanism; the melt entrained relatively few K-feldspar megacrysts, and consequently megacrysts were concentrated around the pocket (Fig. 12a).

(2) High water concentration in the segregated melt caused effective superheating of the melt by lowering its liquidus, destruction of nuclei and resorption of smaller crystals; only the larger solid megacrysts survived (Fig. 12b).

(3) Rapid undercooling of the melt, caused by the lack of nuclei and possibly enhanced by a sudden water-pressure loss and exsolution of the volatile phase, which raised the liquidus temperature; the water-pressure decrease may have been related either to a volcanic eruption or fracturing of the surrounding mostly-crystallized granite. Disequilibrium growth of the orbicules by heterogeneous nucleation on the megacrysts, which acted as nucleation seeds, and crystallization of reversely zoned radial plagioclase and sporadic crystallization of tangential biotite rings according to fluctuations in its saturation (Fig. 12c).

(4) End of orbicular growth and crystallization of the mostly pegmatitic and equiaxial inter-orbicular matrix. The shift from orbicular to equiaxial crystallization occurred when sufficient melt polymerization was attained, possibly related to a critical cooling temperature; it occurred in two stages. Final silica and potassium rich melts crystallized as pegmatite pods and aplites (Fig. 12d).

The time scale of formation of the orbicular granitoid was probably quite fast. The rate of segregation of interstitial melt by filter-pressing is not well constrained, although some rough estimations can be obtained from previous studies; Sisson & Bacon (1999) concluded that 'gas-driven filter pressing can expel melt at velocities of meters to centimeters per year', whereas Bachmann & Bergantz (2004) calculated segregation rates by hindered settling and compaction of ~5 ×

10^{-2} to 5×10^{-3} km^3/yr. A rough calculation using these segregation rates and assuming a volume of ~20 000 m^3 (considering the area of the orbicular granitoid outcrop and a depth of ~20 m) indicates that the 'orbicular melt' could have been segregated in a matter of days. Superheating of the melt and destruction of nuclei can be achieved very rapidly, in a matter of hours, as shown experimentally by Lofgren (1983). Exsolution of water due to pressure release is nearly instantaneous, and consequent undercooling of the melt would be fast (Ort, 1992). Undercooling promotes high growth rates in the order of 10^{-5} to 10^{-7} cm/s for feldspar (e.g. Fenn, 1977; Swanson, 1977; London, 1992). Considering the peak growth rate for plagioclase of ~10^{-6} cm/s obtained by Swanson (1977), the largest radial plagioclase crystals found in the orbicules (~3 cm length) would grow in about 35 days. Thus, orbicule formation could have occurred in a period of a few weeks, in agreement with estimations by Ort (1992) and Decitre, Gasquet & Marignac (2002). This time scale is also in agreement with calculated cooling rates of a few months for pegmatites of similar thickness (e.g. Chakoumakos & Lumpkin, 1990). The inter-orbicular matrix probably crystallized more slowly since it crystallized under more 'normal' conditions, although the mostly pegmatitic texture of the matrix and the pegmatitic pod suggest a pegmatitic environment, and thus also relatively fast crystallization (e.g. London, 2005).

This study highlights some key processes and conditions for the formation of orbicular rocks which have been previously postulated: presence of solids within the melt that act as nucleation seeds; superheating followed by undercooling of the melt; orbicular growth under disequilibrium conditions produced by undercooling of the melt; water concentration and exsolution as a driving force for superheating and undercooling. In addition to these key factors, some other aspects of the proposed genetic model may also be important in the genesis of orbicular rocks: filter-pressing can be a mechanism to segregate the orbicular melt; orbicular rocks can form *in situ* in a mostly closed system; reverse zoning of radial plagioclase can indicate crystallization during undercooling; the shift from orbicular to equiaxial crystallization can occur in more than one stage; orbicule formation can have significant similarities to pegmatite formation. Finally, it is worth noting that the proposed genetic model implies that the K-feldspar megacrysts grew early in the granite magma, an assumption relevant for the ongoing debate concerning the timing of K-feldspar megacryst growth in granites (e.g. Vernon & Paterson, 2008).

Acknowledgements. We greatly appreciate the assistance given by M. Larrovere, F. Morales and F. Sardi during fieldwork. A. Hüber and A. Veit are thanked for help during microprobe measurements. We are grateful to J. de la Rosa for carrying out the whole-rock chemical analyses. J. Otamendi is thanked for reviewing an earlier version of the manuscript. We thank M. Ort, an anonymous reviewer and editor D. Pyle for thorough and helpful reviews. The Consejo Nacional de Investigaciones Científicas y Técnicas (CONICET) and the Deutscher Akademischer Austauschdienst (DAAD) are thanked for scholarships awarded to P. Grosse during his Ph.D. studies. The Consejo de Investigaciones of the Universidad Nacional de Tucumán (CIUNT) is thanked for financial support through project 26/G321.

References

BACHMANN, O. & BERGANTZ, G. W. 2004. On the origin of crystal-poor rhyolites: extracted from batholithic crystal mushes. *Journal of Petrology* **45**, 1565–82.

BEA, F., PEREIRA, M. D., CORRETGÉ, L. G. & FERSHTATER, G. B. 1994. Differentiation of strongly peraluminous, perphosphorus granites. The Pedrobernardo pluton, central Spain. *Geochimica et Cosmochimica Acta* **58**, 2609–28.

BRIGHAM, R. H. 1983. A fluid dynamic appraisal of a model for the origin of comb layering and orbicular structure. *Journal of Geology* **91**, 720–4.

CHAKOUMAKOS, B. C. & LUMPKIN, G. R. 1990. Pressure–temperature constraints on the crystallization of the Harding pegmatite, Taos County, New Mexico. *Canadian Mineralogist* **28**, 287–98.

DECITRE, S., GASQUET, D. & MARIGNAC, C. 2002. Genesis of orbicular granitic rocks from the Ploumanac'h Plutonic Complex (Brittany, France): petrographical, mineralogical and geochemical constraints. *European Journal of Mineralogy* **14**, 715–31.

DEER, W. A., HOWIE, R. A. & ZUSSMAN, J. 1962. *Rock forming minerals, Volume 3: Sheet silicates*. London: Longman, 270 pp.

DE LA ROSA, J. D., CHACÓN, H., SÁNCHEZ DE LA CAMPA, A., CARRASCO, R. & NIETO, J. M. 2001. Metodología y análisis de elementos trazas-REE mediante ICP-MS del standard SARM 1 granito y SARM 4 norita. In *Proceedings of III Congreso Ibérico de Geoquímica*, pp. 435–8. Zaragoza, Spain.

DONALDSON, C. H. 1977. Laboratory duplication of comb layering in the Rhum pluton. *Mineralogical Magazine* **41**, 323–36.

DURANT, D. G. & FOWLER, A. D. 2002. Origin of reverse zoning in branching orthopyroxene and acicular plagioclase in orbicular diorite, Fisher Lake, California. *Mineralogical Magazine* **66**, 1003–19.

ELLISTON, J. N. 1984. Orbicules: An indication of the crystallization of hydrosilicates, I. *Earth Science Reviews* **20**, 265–344.

ENZ, R. D., KUDO, A. M. & BROOKINS, D. G. 1979. Igneous origin of the orbicular rocks of the Sandia Mountains, New Mexico. *Bulletin of the Geological Society of America* **90**, 138–40.

ESKOLA, P. 1938. On the esboitic crystallization of orbicular rocks. *Journal of Geology* **46**, 448–85.

FENN, P. M. 1977. The nucleation and growth of alkali feldspars from hydrous melts. *Canadian Mineralogist* **15**, 135–61.

GALLISKI, M. 1993. La Provincia Pegmatítica Pampeana I: tipología y distribución de sus distritos económicos. *Revista de la Asociación Geológica Argentina* **49**, 99–112.

GOODSPEED, G. E. 1942. Orbicular rocks from Buffalo Hump, Idaho. *American Mineralogist* **27**, 37–47.

GORDILLO, C. E. 1979. Observaciones sobre la petrología de las rocas cordieríticas de la Sierra de Córdoba. *Boletín de la Academia Nacional de Ciencias, Córdoba, Argentina* **53**, 3–44.

GROLIER, J. 1961. Sur le granite orbiculaire de Tissellline (Hoggar, Sahara Central). *Bulletin de la Société Géologique de France* **7**, 174–81.

GROSSE, P., ROSSI, J. N., SARDI, F. G. & TOSELLI, A. J. 2006. Química mineral de los granitos Sanagasta, Huaco y La Chinchilla, Sierra de Velasco, La Rioja, Argentina. In *Proceedings of VIII Congreso de Mineralogía y Metalogenia*, pp. 381–8. Buenos Aires, Argentina.

GROSSE, P., SÖLLNER, F., BÁEZ, M. A., TOSELLI, A. J., ROSSI, J. N. & DE LA ROSA, J. D. 2009. Lower Carboniferous post-orogenic granites in central-eastern Sierra de Velasco, Sierras Pampeanas, Argentina: U–Pb monazite geochronology, geochemistry and Sr–Nd isotopes. *International Journal of Earth S ciences* **98**, 1001–25.

HIGGINS, M. 1999. Origin of megacrysts in granitoids by textural coarsening: a crystal size distribution (CSD) study of microcline in the Cathedral Peak Granodiorite, Sierra Nevada, California. In *Understanding granites: integrating new & classical techniques* (eds A. Castro, C. Fernández & J. L. Vigneresse), pp. 207–19. Geological Society of London, Special Publication no. 168.

HORT, M. 1998. Abrupt change in magma liquidus temperature because of volatile loss or magma mixing: effects on nucleation, crystal growth and thermal history of the magma. *Journal of Petrology* **39**, 1063–76.

HUNT, J. D. 1984. Steady state columnar and equiaxed growth of dendrites and eutectic. *Materials Science and Engineering* **65**, 75–83.

LAHTI, S. 2005. *Orbicular rocks in Finland*. Espoo: Geological Survey of Finland, 177 pp.

LEVESON, D. J. 1963. Orbicular rocks of the Lonesome Mountain area, Beartooth Mountains, Montana and Wyoming. *Bulletin of the Geological Society of America* **74**, 1015–40.

LEVESON, D. J. 1966. Orbicular rocks: A review. *Bulletin of the Geological Society of America* **77**, 409–26.

LINARES, E. & QUARTINO, B. J. 1978. Nuevas aportaciones a la génesis de las rocas orbiculares de La Rioja y el control recíproco de datos K–Ar e interpretación petrogenética. In *Proceedings of VII Congreso Geológico Argentino* **2**, 585–93. Neuquén, Argentina.

LINDH, A. & NÄSSTRÖM, H. 2006. Crystallization of orbicular rocks exemplified by the Slättemossa occurrence, southeastern Sweden. *Geological Magazine* **143**, 713–22.

LOFGREN, G. E. 1974*a*. An experimental study of plagioclase crystal morphology: isothermal crystallization. *American Journal of Science* **274**, 243–73.

LOFGREN, G. E. 1974*b*. Temperature induced zoning in synthetic plagioclase feldspar. In *The Feldspars* (eds W. S. McKenzie & J. Zussman), pp. 362–75. Manchester: University of Manchester Press.

LOFGREN, G. E. 1983. Effect of heterogeneous nucleation on basaltic textures: A dynamic crystallization study. *Journal of Petrology* **24**, 229–55.

LOFGREN, G. E. & DONALDSON, C. H. 1975. Curved branching crystals and differentiation in comb-layered rocks. *Contributions to Mineralogy and Petrology* **49**, 309–19.

LONDON, D. 1992. The application of experimental petrology to the genesis and crystallization of granitic pegmatites. *Canadian Mineralogist* **30**, 499–540.

LONDON, D. 2005. Granitic pegmatites: an assessment of current concepts and directions for the future. *Lithos* **80**, 281–303.

LONDON, D., MORGAN, G. B. & HERVIG, R. L. 1989. Vapor-undersaturated experiments with Macusani glass + H_2O at 200 MPa, and the internal differentiation of granitic pegmatites. *Contributions to Mineralogy and Petrology* **102**, 1–17.

MARSH, B. D. 1988. Crystal size distribution (CSD) in rocks and the kinetics and dynamics of crystallization I. Theory. *Contributions to Mineralogy and Petrology* **99**, 277–91.

MARSH, B. D. 1996. Solidification fronts and magmatic evolution. *Mineralogical Magazine* **60**, 5–40.

MARTORANO, M. A. & BISCUOLA, V. B. 2009. Predicting the columnar-to-equiaxed transition for a distribution of nucleation undercoolings. *Acta Materialia* **57**, 607–15.

MCBIRNEY, A. R. & NOYES, R. M. 1979. Crystallization and layering of the Skaergaard intrusion. *Journal of Petrology* **20**, 487–554.

MOORE, J. G. & LOCKWOOD, J. P. 1973. Origin of comb layering and orbicular structure, Sierra Nevada batholith, California. *Bulletin of the Geological Society of America* **84**, 1–20.

NAKAMURA, N. 1974. Determination of REE, Ba, Mg, Na and K in carbonaceous and ordinary chondrites. *Geochimica et Cosmochimica Acta* **38**, 757–73.

ORT, M. H. 1992. Orbicular volcanic rocks of Cerro Panizos: their origin and implications for orb formation. *Bulletin of the Geological Society of America* **104**, 1048–58.

OWEN, J. V. 1991. Significance of epidote in orbicular diorite from the Grenville Front zone, eastern Labrador. *Mineralogical Magazine* **55**, 173–81.

PROPACH, G. 1976. Models of filter differentiation. *Lithos* **9**, 203–9.

QUARTINO, B. J. & VILLAR FABRE, J. 1962. El cuerpo granítico orbicular precámbrico de la Pampa de Los Altos, sierra de Velasco. *Revista de la Asociación Geológica Argentina* **18**, 11–41.

RAPELA, C. W., BALDO, E. G., PANKHURST, R. J. & SAAVEDRA, J. 2002. Cordieritite and leucogranite formation during emplacement of highly peraluminous magma: the El Pilón Granite Complex (Sierras Pampeanas, Argentina). *Journal of Petrology* **43**, 1003–28.

SARDI, F. G. 2005. Petrografía y caracterización de la mena del Distrito Pegmatítico Velasco, La Rioja, Argentina. *Proceedings of XVI Congreso Geológico Argentino* **5**, 231–8. La Plata, Argentina.

SARDI, F. G. & GROSSE, P. 2005. Consideraciones sobre la clasificación del Distrito Velasco de la Provincia Pegmatítica Pampeana, Argentina. In *Proceedings of XVI Congreso Geológico Argentino* **5**, 239–42. La Plata, Argentina.

SEDERHOLM, J. 1928. On orbicular granites, spotted and nodular granites, etc., and the rapakivi texture. *Bulletin de la Commission Géologique de Finlande* **83**, 1–105.

SINCLAIR, W. D. & RICHARDSON, J. M. 1992. Quartz-tourmaline orbicules in the Seagull batholith, Yukon Territory. *Canadian Mineralogist* **30**, 923–35.

SIQUEIRA, C. A., CHEUNG, N. & GARCIA, A. 2002. Solidification thermal parameters affecting the columnar-to-equiaxed transition. *Metallurgical and Materials Transactions A* **33**, 2107–18.

SISSON, T. W. & BACON, C. R. 1999. Gas-driven filter pressing in magmas. *Geology* **27**, 613–16.

SÖLLNER, F., GROSSE, P., GERDES, A., TOSELLI, A. J. & ROSSI, J. N. 2009. U–Pb LA-ICP-MS age determinations of growth impulses in zircons from Carboniferous post-orogenic granites, Sierra de Velasco

(NW-Argentina). In *Proceedings of XXI Colloquium on Latin American Earth Sciences*, pp. 267–70. Göttingen, Germany.

SUREDA, R. & VIRAMONTE, J. 1972. El granito orbicular del Cerro Reventón, Sierra de Los Comechingones, Córdoba. In *Proceedings of V Congreso Geológico Argentino*, pp. 215–40. Carlos Paz, Argentina.

SWANSON, S. E. 1977. Relation of nucleation and crystal growth rate to the development of granite textures. *American Mineralogist* **62**, 966–78.

SYMES, R. F., BEVAN, J. C. & QASIM, J. M. 1987. The nature and origin of orbicular rocks from near Deshai, Swat Kohistan, Pakistan. *Mineralogical Magazine* **51**, 635–47.

TAGIRI, M., OBA, T. & FUJINAWA, A. 2007. Radial cordierite-bearing orbicular granite formed from the melting of metapelitic hornfels in granitic magma, Tsukuba Mountains, Japan. *Journal of Mineralogical and Petrological Sciences* **102**, 127–36.

TISCHENDORF, G., FÖRSTER, H.-J. & GOTTESMANN, B. 1999. The correlation between lithium and magnesium in trioctahedral micas: improved equations for Li_2O estimation from MgO data. *Mineralogical Magazine* **63**, 57–74.

TISCHENDORF, G., GOTTESMANN, B., FÖRSTER, H.-J. & TRUMBULL, R. B. 1997. On Li-bearing micas: estimating Li from electron microprobe analyses and an improved diagram for graphical representation. *Mineralogical Magazine* **61**, 809–34.

VERNON, R. H. 1985. Possible role of superheated magma in the formation of orbicular granitoids. *Geology* **13**, 843–45.

VERNON, R. H. 1986. K-feldspar megacrysts in granites: phenocrysts, not porphyroblasts. *Earth-Science Reviews* **23**, 1–63.

VERNON, R. H. & PATERSON, S. R. 2008. How late are K-feldspar megacrysts in granites? *Lithos* **104**, 327–36.

VILLASECA, C. & BARBERO, L. 1994. Chemical variability of Al–Ti–Fe–Mg minerals in peraluminous granitoid rocks from Central Spain. *European Journal of Mineralogy* **6**, 691–710.

YAZGAN, E. & MASON, R. 1988. Orbicular gabbro from near Baskil, southeastern Turkey. *Mineralogical Magazine* **52**, 161–73.